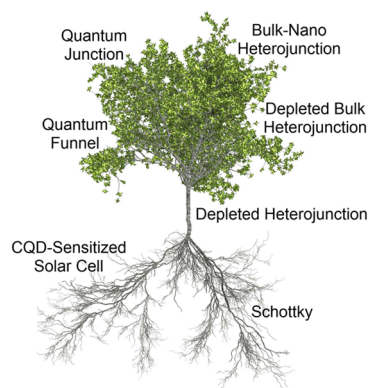


The Architecture of Colloidal Quantum Dot Solar Cells: Materials to Devices

Illan J. Kramer and Edward H. Sargent*

Edward S. Rogers Department of Electrical & Computer Engineering, University of Toronto, 10 King's College Road, Toronto, Ontario M5S 3G4, Canada



CONTENTS

1. Introduction	863
2. Measuring and Modeling CQD Solar Cells	863
2.1. Solar Cell Characterization Considerations	864
2.2. Drift Transport and the Depletion Region	865
2.3. Diffusion and Recombination	865
2.4. Interfaces between CQDs and Electrodes	866
3. CQD-Sensitized Solar Cells	867
4. Schottky CQD Solar Cells	867
5. Depleted Heterojunction CQD Solar Cells	869
6. CQD Solar Cells Using Quantum Funnel	871
7. Depleted Bulk Heterojunction CQD Solar Cells	873
8. Bulk–Nano Heterojunction CQD Solar Cells	874
9. Quantum Junction Solar Cells	874
10. Multiple-Junction CQD Solar Cells	875
11. Hot-Carrier Effects in CQD Materials: Device Implications	876
11.1. Hot-Electron Transfer	876
11.2. Multiple Exciton Generation	877
12. Conclusions	877
Author Information	878
Corresponding Author	878
Author Contributions	878
Notes	878
Biographies	878
Acknowledgments	878
Abbreviations	878
References	879

1. INTRODUCTION

Colloidal quantum dots (CQDs) are nanometer-sized particles of semiconductor dispersed in a solvent with the aid of a stabilizing ligand. CQDs' physical dimensions and shape dictate their optical and electrical properties.¹ This size-effect tunability

differentiates them from other, non-quantum-confined nanocrystals, providing a versatile framework on which to build a multitude of optoelectronic devices. Control over CQD size, ligand chemistry, and annealing conditions have enabled many recent advances in the properties and performance of solution-processed solar cells, photodetectors,^{2–4} and light-emitting devices (LEDs).^{5,6}

This review focuses in particular on energy harvesting applications of CQDs. Photovoltaics leverage materials' low-cost solution processing while exploiting their broad spectral tunability matched to the Sun's wide spectrum. A growing community of engineering, chemistry, physics, and materials science researchers are pursuing the development of CQD solar cells with the goal of achieving high efficiency at low cost.

We focus in particular on the device architectures, and the enabling materials chemistry advances, that have enabled solar cells employing CQDs as the primary active layer to see rapid advances in solar power conversion efficiency. Each architecture presented herein builds upon the improvements of each previous generation, thus representing a “family tree” of solar cell devices (Figure 1), not a set of distinct, stand-alone advances. This review therefore complements excellent recent reviews that survey the CQD field from the point of view of chemical synthesis and CQD film processing⁷ as well as photophysics.⁸

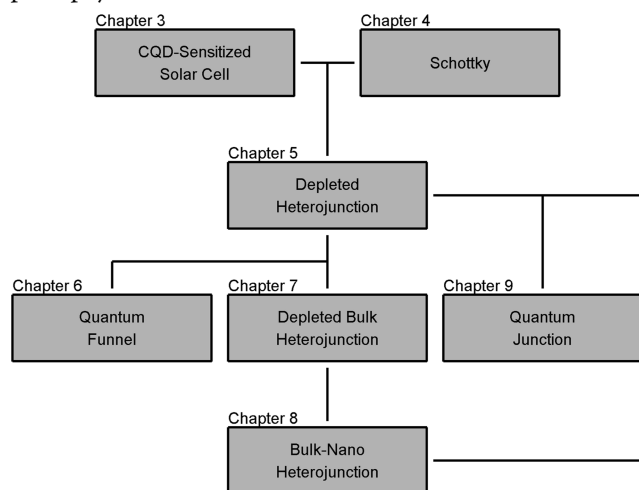


Figure 1. Family tree of colloidal quantum dot photovoltaic device architectures.

Received: May 31, 2013

Published: September 20, 2013

2. MEASURING AND MODELING CQD SOLAR CELLS

The photocurrent in solar cells can be produced from the drift of charge carriers in an electric field, and also from the diffusion of photocarriers. Typical silicon p–n junction solar cells include both a comparatively thin depletion region in which a built-in field drives drift transport; as well as a much thicker quasineutral region that exploits the long minority carrier diffusion length, L ($L = (\tau D)^{1/2}$, where τ is the carrier lifetime and D is the diffusivity) in this indirect-bandgap, long electron–hole pair lifetime, medium (Figure 2a).⁹ High free carrier

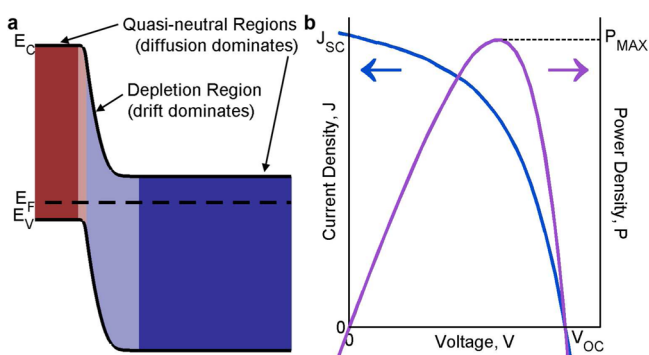


Figure 2. (a) p–n junction solar cell with both a depletion region and quasineutral regions. (b) Typical J – V (blue curve, left axis) and P – V (violet curve, right axis) characteristics of a solar cell.

mobilities and low defect densities enable extraction of photogenerated carriers from these quasineutral regions through a highly efficient diffusion processes. p–i–n solar cells, in contrast, rely heavily on a distributed electric field through a thick intrinsic layer within the absorbing medium, be it amorphous silicon^{9–12} or microcrystalline silicon.¹³ p–i–n solar devices are dominated by drift current and provide a particularly relevant exemplar in the analysis of CQD solar cells.

2.1. Solar Cell Characterization Considerations

In order to consider the implications of using CQD films as the active layer in a solar cell, it is important to understand how solar cells are characterized. Figure 2b shows a typical J – V and P – V characteristic curve of a photovoltaic device. Device efficiency, η , is defined by eq 1

$$\eta = \frac{P_{\text{max,ELEC}}}{P_{\text{IN,OPT}}} = \frac{\max(J \cdot V)}{P_{\text{IN,OPT}}} \quad (1)$$

where $P_{\text{MAX,ELEC}}$ is the maximum electrical power density generated, J is the current density, V is the applied voltage, and $P_{\text{IN,OPT}}$ is the incident optical power density. At AM 1.5 G conditions, $P_{\text{IN,OPT}}$ is 100 mW/cm².¹⁴ The fill factor, FF, is an additional figure of merit and is defined as $P_{\text{MAX,ELEC}} / (J_{\text{SC}} V_{\text{OC}})$, where J_{SC} and V_{OC} are the current density at short-circuit conditions and voltage at open-circuit conditions, respectively. The fill factor can be understood to quantify the cell's ability to continue to extract current even as the band bending is reduced; this condition is realized as the device approaches the maximum power point in the direction of V_{OC} under a forward-like applied bias. Graphically, it is a measure of the “squareness” of the J – V curve.

Also affecting the fill factor of the device are the parasitic series, R_{S} , and shunt, R_{SH} , resistances. From the J – V curve, R_{S} is the inverse of the J – V slope at V_{OC} , while R_{SH} is the inverse of the J – V slope at J_{SC} (this is strictly only true for values of R_{SH}

$\gg R_{\text{S}}$).⁹ For high performing solar cells, R_{S} should approach 0, while R_{SH} should approach ∞ .

For active materials such as CQD films where $1/\alpha$, where α is the absorption coefficient, is of the same order as the free carrier extraction length, external quantum efficiency (EQE) measurements have proved useful in profiling the effectiveness of each nanometer of device thickness at extracting photogenerated carriers. PbS and PbSe CQD films fall into this category, with both free carrier dependent depletion widths and diffusion lengths between ~ 30 and ~ 400 nm,^{15–17} and complete above-bandgap absorption at < 1 μm film thickness.^{18,19}

EQE, also known as the incident photon conversion efficiency (IPCE), is defined by eq 2

$$\text{EQE} = \frac{J_{\text{SC}}}{\Phi_{\text{IN}} \cdot e} \cdot 100\% = \frac{J_{\text{SC}}}{P_{\text{IN}} \cdot e} \cdot \frac{hc}{\lambda} \cdot 100\% \quad (2)$$

$$\text{IQE} = \frac{\text{EQE}}{\text{abs}\%} \quad (3)$$

where Φ_{IN} is the incident photon flux, P_{IN} is the incident monochromatic optical power density, h is Planck's constant, c is the speed of light, λ is the monochromatic wavelength, and e is the elementary charge. While the EQE provides insight into how individual wavelengths are converted into electrical current, it does not distinguish between the cocontributing factors of absorption and extraction. The internal quantum efficiency, IQE (also known as absorbed photon conversion efficiency, APCE), more closely approximates extraction efficiency by dividing the EQE by the fraction of photon current absorbed at each wavelength (eq 3). The absorbed light considered in the IQE calculation takes into account both reflective and transmissive losses outside of the active layer. As these parasitic optical losses become nontrivial, the IQE deviates from reporting the pure extraction efficiency.

Integrating the product of the measured EQE spectrum with the AM 1.5 G spectrum in a manner similar to Henry's analysis on the total AM 1.5 G spectrum²⁰ allows determination of an expected J_{SC} for reconciliation with the measured value under AM 1.5 G conditions.

When characterizing solar cells, several important factors need to be taken into consideration. First, the lamp spectrum and its relationship to the true AM 1.5 G spectrum needs to be quantified in the form of a spectral mismatch factor by which measured current should be scaled.²¹ This includes understanding the spectral response of both the calibrated solar cell used for confirming AM 1.5 G intensity and of the solar cell under test. Second, the aperturing of the device is crucial since, unlike in crystalline semiconductors, lateral carrier collection is negligible.²² The device area should therefore be defined as the illuminated area, and it should be less than or equal to the physical top contact size. Only when the physical contacts are patterned, isolating them from the underlying substrate, can the device be illuminated without an aperture. Unmasked exposure areas can lead to edge effects that effectively increase the active area of the device, yielding falsely high currents. This effect is exacerbated for very small device areas where the relative impact of the edge is more pronounced. For this reason, efficiency results for very small devices should be taken with caution.

2.2. Drift Transport and the Depletion Region

In organic photovoltaics, dye-sensitized solar cells, and CQD photovoltaics, a carrier extraction length is often defined as $W_{\text{DEP}} + L_{\text{DIFF}}$, where W_{DEP} is the width of the depletion region and L_{DIFF} is the minority carrier diffusion length in the active material.

This extraction length can often be much less than the absorption length ($1/\alpha$) of the most weakly absorbed above-bandgap optical wavelength of interest. The result is a compromise between the absorption of light and the extraction of photocharges.

This compromise can be overcome using bulk heterojunctions²³ and Grätzel cell²⁴ high-surface-area electrodes.¹⁶ This has been particularly true of solar cells in which CQDs are used as sensitizers, adsorbed as a monolayer onto a high-surface-area electrode.^{25–30}

Nevertheless, many advances in CQD photovoltaics have relied on CQD films, in which photocharges must travel significant distances (many quantum dots) within the CQD film itself.

This has required the development of models to describe phenomena such as drift and diffusion, electric fields and carrier concentration gradients, generation and recombination, and transport and trapping in CQD solids.^{31–33} In this picture, the CQD film is treated as a bulk semiconductor whose bandgap is determined by the quantum-tuned nanoparticles, and electron affinities, ionization potentials, Fermi and quasi-Fermi levels, average electron and hole mobilities, an average dielectric constant (and, in the optical regime, average n and k parameters), and average generation and recombination rates are all measured and modeled. The successful treatment of these films as classical semiconductors suggests the Shockley–Queisser power conversion efficiency limit³⁴ for conventional p–n solar cells can be translated to CQD solar cells.^{35,36}

In such a picture, semiconductor theory holds that a depletion region is formed when two noninsulating, non-metallic, differently doped solids are placed in electrical contact with each other. The widths of these depletion regions on either side of this junction, W_1 and W_2 , are derived according to eqs 4 and 5, respectively.³⁷

$$W_1 = \sqrt{\frac{2N_{A2}\epsilon_1\epsilon_2(\Psi_{\text{bi}} - V)}{qN_{D1}(\epsilon_1N_{D1} + \epsilon_2N_{A2})}} \quad (4)$$

$$W_2 = \sqrt{\frac{2N_{D1}\epsilon_1\epsilon_2(\Psi_{\text{bi}} - V)}{qN_{A2}(\epsilon_1N_{D1} + \epsilon_2N_{A2})}} \quad (5)$$

In these equations, it is assumed that side 1 of the junction is n-type, and therefore has a free electron density of $n = N_{D1}$ and permittivity of ϵ_1 , while side 2 is p-type and therefore has a free hole density of $p = N_{A2}$ and permittivity of ϵ_2 . Ψ_{bi} represents the built-in potential of the junction, while V represents any applied bias. These expressions apply equally well to heterojunctions and homojunctions.

While excitonic transport (i.e., a model in which tightly bound electron–hole pairs diffuse together, hopping from CQD to CQD until reaching some charge separating interface) has been postulated as a relevant transport mechanism in CQD solids,³⁸ it has also been shown that excitons readily dissociate in CQD solids when an electric field is present³⁹ (and even in the absence of an electric field⁴⁰). The successful harvesting of photocharges from a CQD layer of >200 nm, a thickness much

greater than the (downhill) excitonic diffusion mechanism is predicted to support,¹⁵ is consistent with this picture of rapid dissociation of excitons and subsequent collection of the resultant free electrons and holes in the presence of an electric field, and thus supports the effective medium picture. Needless to say, the model employs quantitative parameters, especially mobilities, that are very different (in the case of mobilities, 10^{-4} – 10^1 cm²/V s for CQDs^{16,41,42}) than those of their bulk counterparts (10^2 – 10^5 cm²/V s⁴³).

This picture offers specific guidance in solar cell optimization. As one example, increasing the doping in an n-type electrode that forms a depletion region in an adjacent p-type light-absorbing CQD solid enables a deeper depletion region to be formed in the CQD material. In a similar vein, high doping of the CQD solid shrinks the depletion region within this heavily doped film, harming EQE and the resultant current density. This picture explains the recent success of asymmetrical doping of CQD solar cells.^{44,45} Naturally, the picture also reinforces the crucial importance of continued progress in increasing the minority carrier diffusion length, under 1 Sun conditions, to enable efficient extraction of charge carriers generated in a quasineutral portion of the CQD active region.

Because CQD films have the added complications of being made of variable-sized constituent material building blocks as well as being deposited from solution, the nature of charge transport through the films can also be size-dependent^{46,47} and matrix (or ligand)-dependent.^{48–52} Even nanoparticle shape influences electronic behavior.^{53–56} Efforts are underway toward achieving the type of three-dimensional periodicity ubiquitous in crystalline semiconductor lattices.^{57–67} The ultimate hope is that these superlattices, made up of one or several building block nanocrystals, have more reproducible and uniform optical and electrical properties than their irregular counterparts,^{68,69} an analogue to single-crystal semiconductor lattices made from colloidal quantum dots, the latter sometimes referred to as artificial atoms.

A further consideration when working with these quantum-confined nanoparticles is the evolution of their size and shape, particularly under illumination. Photooxidation can convert some of the semiconductor material into an insulating oxide. The resulting quantum dot has effectively smaller dimensions, increasing its bandgap.^{70,71} Notably, this instability⁷² is also size-dependent.⁷³ Large CQDs, those over 4 nm in diameter, are more prone to photooxidation than their smaller counterparts. This may explain the higher open-circuit voltage stability of a variety of CQD solar cells employing larger bandgap CQDs.^{74–78} Beyond changing the optical characteristics of the dots, the evolution of these insulating shells reduces the overlapping wave functions of adjacent dots, thereby reducing dot-to-dot coupling.

2.3. Diffusion and Recombination

Electronic traps play a critical role in semiconductors, be they classical or excitonic. Deep traps act as recombination centers, capturing an electron and a hole and ultimately leading to their recombination. Shallow traps associated with a given band retard the egress of that charge carrier, capturing it into a low-mobility state as it travels along its path.³² It is thus not surprising that increases in CQD film mobilities have been achieved through improved passivation techniques,^{7,41,49,67,79} as observed using field-effect transistors (FETs). These observations are consistent with the fact that hopping^{42,46–48,80–83} transport, where the relative energies of and distances between

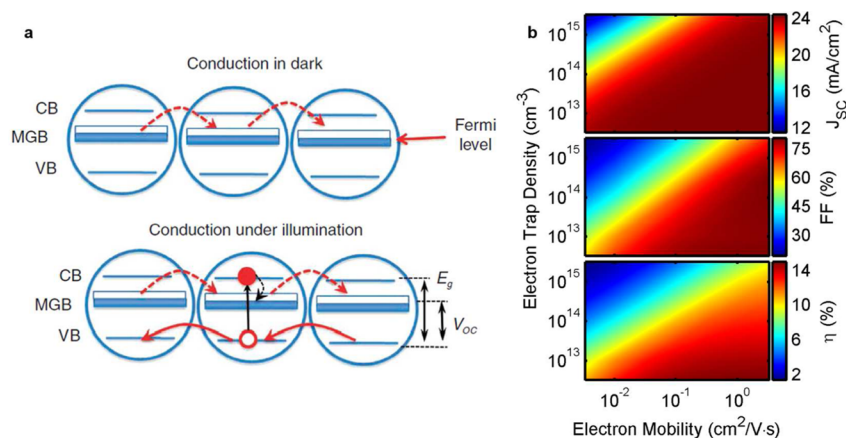


Figure 3. (a) Transport mechanisms in CQD films in the dark (top) and under illumination (bottom) illustrate how traps mediate transport and define the extent of quasi-Fermi level splitting in CQD films with high defect densities, and specifically in optoelectronic devices. This framework is particularly relevant to CQD solar cells, where this concept, in tandem with an appropriate device architecture, can provide an upper bound on V_{OC} that is substantially less than the optical bandgap of the material with that cell architecture would imply. Reprinted by permission from Macmillan Publishers Ltd.: *Nature Communications* (ref 91), copyright 2011. (b) Modeled diagonal equivalency of traps and mobility on solar cell figures of merit. Reprinted with permission from ref 32. Copyright 2011 American Chemical Society.

localized states determine the ability of charges to progress through the film, has been reported in the preponderance of CQD films successfully deployed in photovoltaic devices.

While the transport mechanism is clearly important for understanding current extraction in a solar cell, simply increasing a parameter such as mobility is insufficient. In a high defect density paradigm, increasing mobility merely speeds up the ability for a free carrier to find a defect. Recombination rate at defects is therefore directly proportional to mobility.⁴² Instead, reducing the number of recombination centers^{32,67,75,84–90} and improving the monodispersity^{42,48,85} of the CQD populations provide a path toward improved current collection.

Traps have received much attention in CQD films recently, including characterizations of their density⁸⁵ and depth⁹¹ within the bandgap. Figure 3a illustrates how a midgap band of traps (MGB) influences the transport while pinning the Fermi level of the film.

The CQD films employed in the various architectures discussed in this review are deposited from solution and postprocessed with nonsolvents (such as methanol) and/or highly reactive ligands (such as EDT and MPA). These solid-state treatments leave the individual quantum dots vulnerable to oxidation⁷⁵ or subject to physical reorganization.⁸⁷ Crystal or surface defects manifest as electronic trap states where recombination is likely to occur, reducing both extractable current and attainable voltage.

The impact of traps on CQD solar cells has been modeled^{32,92} and observed experimentally.^{44,92,93} Figure 3b shows how, within the low-to-moderate defect density paradigm, decreasing trap density exhibits a diagonal equivalency to increasing mobility for solar cell performance.³² These both result in an increased diffusion length: the reduced electron trap density increases carrier lifetime, τ , while the higher mobility increases the diffusivity, D , through the Einstein relation.³⁷

Characterization of these traps (their depth within the bandgap, their density, the shape of their distribution, etc.) in CQD films has been a field of great advance in recent years.^{44,88,89,94}

In addition to the delicacy of the surface properties of each individual CQD, these CQD solutions have a finite population size distribution. Despite colloidal quantum dots having a much higher degree of monodispersity than their epitaxial growth or chemical bath deposited counterparts,²⁵ they do nevertheless exhibit sufficient polydispersity that the ensemble bandgap of a disordered CQD film does not have sharp edges.⁹⁵ If these Urbach tails⁹⁶ extend well into the bandgap, carriers will eventually funnel to the smallest bandgap CQDs within the film where they will recombine.^{97–100} While this clearly has an impact on current collection, there is also an implication for voltage. The presence of a high degree of polydispersity would pin the quasi-Fermi level within the film to the smallest bandgap, rendering the nominal “bulk” bandgap wasteful.⁸⁵ For current deep trap densities in the 10^{16} to 10^{17} cm^{-3} range, polydispersity plays only a small role in limiting performance, but as trap densities are reduced, CQD films may enter a polydispersity-limiting regime.

As seen in Figure 4, surface traps and these so-called “quantum traps” (i.e., small-bandgap CQDs or aggregates of large-bandgap CQDs within a matrix of larger-bandgap CQDs) have recently been considered on an even footing; trap depth (E_t), trap density (N_t), and CQD size standard deviation (σ) can be explored and impact relative to surface trap density distributions quantitatively compared.

2.4. Interfaces between CQDs and Electrodes

As in all semiconductor devices, interfaces play an important role in CQD solar cells. These have been addressed in another recent review,¹⁰¹ but will briefly be discussed here as well. Whereas the preceding two sections delved into transport of carriers through a CQD film, injection of electrons and holes from the CQD film into adjacent phases can have just as big an impact on photovoltaic efficiency.

In the same spirit as section 2.3, interfacial defects such as lattice strain and dangling bonds can result in recombination centers that pin the quasi-Fermi levels and scavenge current-carrying charge carriers.¹⁰²

Beyond recombination centers, interfaces can also mediate the efficiency with which charges inject from one material into another. By tuning the conduction or valence band offsets

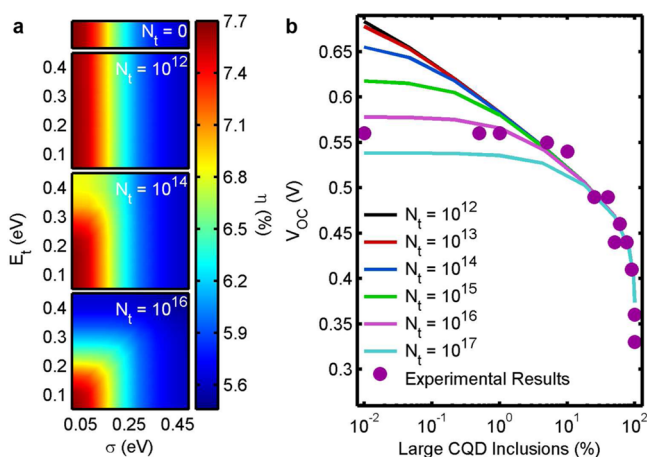


Figure 4. (a) Modeled η as functions of N_t (trap density, rows 1–4, in units of cm $^{-3}$), E_t (trap depth, vertical axes), and σ , the standard deviation of CQD sizes, in units relating to bandgap (horizontal axes). (b) Modeled and experimental V_{OC} as a function of trap density (curves) and polydispersity (horizontal axis). Reprinted with permission from ref 85. Copyright 2012 American Chemical Society.

between the layers adjacent to deposited CQDs, forward injection of charges from the CQDs can be much more than, much less than, or comparable to back injection into the CQDs.¹⁰³

These considerations become particularly important when CQDs are deposited on a highly structured scaffold as in sensitized architectures.^{25,104} Often present in monolayers or even submonolayers, each CQD sees multiple interfaces, often sandwiched between two materials, one responsible for collecting electrons, the other for collecting holes. The energetics of these interfaces must be finely adjusted to ensure that electrons injected into the electron acceptor are extracted prior to encountering a hole in the hole-transport layer. Any back injection of carriers, typically in regions without complete monolayer coverage of CQDs, reduces device shunt resistance and thus degrades fill factor.

3. CQD-SENSITIZED SOLAR CELLS

The earliest reports of solar cells employing CQDs only used the CQDs to compliment absorption by other, non-quantum-confined materials.^{77,105,106} The first report of a solar cell using CQDs as the primary absorber in a solar cell appeared in 1998 and used InP CQDs as sensitizers in a dye-sensitized solar cell (DSSC) configuration.¹⁰⁷ This architecture offered high voltage and featured absorption of light on the rectifying side of the device.

In these devices, known as CQD-SSCs, a monolayer of CQDs coat a transparent, nanoporous electron acceptor such as TiO $_2$ or ZnO. This highly structured interface is then infiltrated by an electrolyte for hole extraction. Through the highly structured electron acceptor coated with CQDs, high absorption can be combined with excellent extraction to achieve high efficiency. A 2007 report showed vertically oriented ZnO nanowires sensitized with CdSe CQDs and infiltrated with an iodine-based liquid electrolyte (Figure 5).¹⁰⁸

The shunt resistance was notable in particular and appears to be symptomatic in other instances of CQD-SSC devices.^{109–111} Due to the large CQD diameter (relative to the nanoporous titania pore diameter), forming a continuous monolayer overcoating the entire nanoporous electron acceptor very

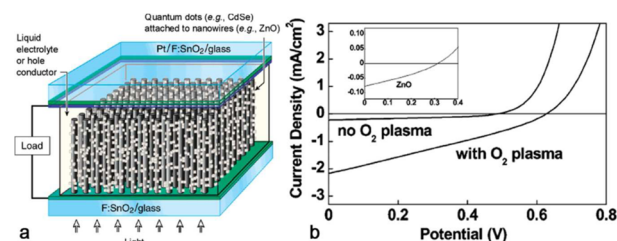


Figure 5. (a) Schematic diagram and (b) photovoltaic performance of ZnO nanowire CQD-sensitized solar cells. Reprinted with permission from ref 108. Copyright 2007 American Chemical Society.

difficult; in fact as little as 14% of the TiO $_2$ surface may be covered by CQDs.¹¹² The uncoated surfaces of the TiO $_2$ or ZnO electron acceptors become free to form soft shorts with the hole-transporting electrolyte (i.e., the shunt resistance drops dramatically, but not to a true short, due to direct but spatially infrequent contact between the electron and hole-transporting phases), resulting in low shunt resistance in the absence of other titania passivation techniques. A high degree of dye loading in DSSCs using molecular dyes ensures large shunt resistances and obviates the need for additional titania surface passivation. Exchanging the bulky ligands required to maintain colloidal stability in solution with shorter bifunctional ligands designed to tether the CQDs to the titania electrode has improved CQD loading.^{113,114} This route offers the most direct route to improved performance within the CQD-SSC architecture as was recently shown by improving the loading factor to 34% through prefunctionalizing the CQDs with the appropriate final ligand without the need for additional ligand chemistry at the interface between the TiO $_2$ and CQD.²⁷

An alternatively interesting strategy involves presensitizing colloidal stable titania nanoparticles and then depositing the rectifying assembly at once.¹¹⁵

Ultimately, with weaker absorption per unit length than dye molecules, thicker nanoporous electrodes must be employed for sensitization with CQDs in order to absorb all the incident light. Thicker electrodes directly add to the series resistance as electrons have further to travel in the electron acceptor and holes have further to travel in the electrolyte. These thicker electrodes also become more difficult to fully infiltrate since deposition of CQDs is typically done through a soaking procedure and therefore from the top down.

While some promising results have been achieved through the CQD-SSC architecture ($\eta = 1.8\%$ ¹¹⁶ to 2.9% ¹¹⁰ and more recently $\eta > 5\%$ ²⁷), the deposition of high-quality presynthesized CQDs into a nanoporous matrix remains a challenge for the materials chemistry community. Research into sensitizing nanoporous TiO $_2$ with quantum dots has largely shifted toward chemical bath deposition (CBD)^{117–121} or successive ionic layer adsorption and reaction (SILAR) of quantum dots,^{114,122} wherein the quantum dot nucleation and synthesis occurs at the same time as deposition rather than beforehand (as with storage in a colloidal stable solution). Great strides have been made using the SILAR method to achieve greater than 5% efficiency.^{123,124} A remaining challenge in this approach is to improve optical properties, and monodispersity, in these in situ synthesized quantum dots.²⁵

4. SCHOTTKY CQD SOLAR CELLS

The first report of a solar cell using a thin film assembly of CQDs as the primary absorber appeared in 2005.¹²⁵ These

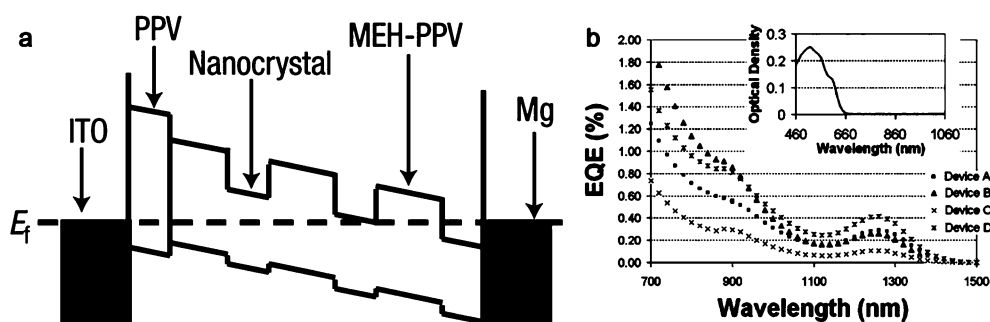


Figure 6. (a) Band diagram of polymer/CQD solar cell. Reprinted by permission from Macmillan Publishers Ltd.: *Nature Materials* (ref 125), copyright 2005. (b) External quantum efficiency of P3OT/PbS CQD bilayers (A, B, and C) and pure PbS CQD (D) devices with optical density of PbS CQDs employed (inset). Reprinted with permission from ref 126. Copyright 2005 AIP Publishing LLC.

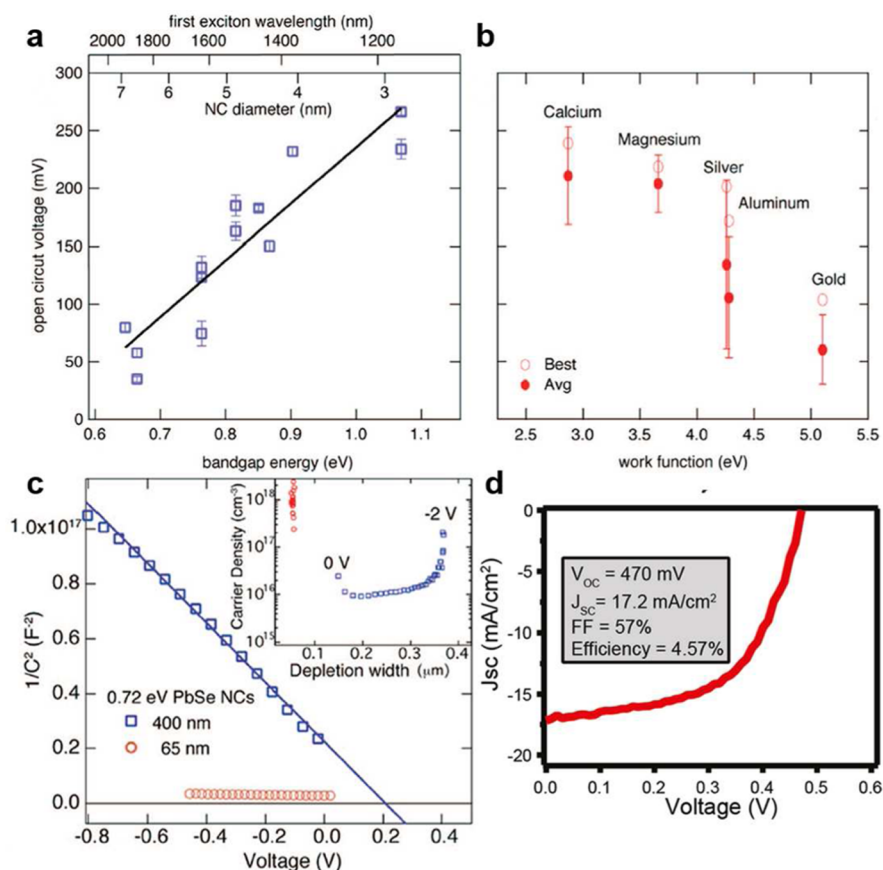


Figure 7. V_{OC} as a function of (a) CQD size (and thus bandgap energy and first excitonic wavelength) and (b) Schottky contact work function. (c) Mott-Schottky analysis of PbSe CQD films of 65 and 400 nm thicknesses. Reprinted with permission from ref 131. Copyright 2008 American Chemical Society. (d) J - V curves of champion Schottky CQD solar cell exhibiting V_{OC} of 0.47 V and η of 4.57%. Reprinted with permission from ref 134. Copyright 2011 American Chemical Society.

solar cells relied on electron affinity differences between the transparent conductive oxide (TCO), in this case indium tin oxide (ITO) and the reflective back contact (Mg), to produce a built-in field driving extraction of electrons (through the dot phase) and holes (through the polymer phase) in their respective directions (Figure 6a).

These cells primarily utilized PbS CQDs and blended them with the organic polymer, poly[2-methoxy-5-(2-ethylhexyloxy)-1,4-phenylenevinylene] (MEH-PPV), to absorb light and separate the photogenerated electron-hole pair through conduction band offsets. The electronic impact of the polymer was subsequently further explored¹²⁶ and, compared to

improved hole transport in CQD solids, was in fact found to impede hole extraction. Figure 6b illustrates the EQE of a set of devices, wherein devices A, B, and C employ the organic polymer poly(3-octylthiophene-2,5-diyl) (P3OT) coated with varying thicknesses of PbS CQDs and device D employs only PbS CQDs of the same thickness as device A with no additional polymer.

The advent of polymer-free CQD devices confirmed that the separation, and ensuing separate transport of electrons and holes, can proceed efficiently in pure CQD films, in the presence of an electric field. This insight opened the possibility of devices based on suitably engineered CQD films alone, and

turned the field in a direction more akin to polycrystalline inorganic semiconductors, except with the added benefit of quantum-tuned bandgaps.

This picture enabled the development of Schottky CQD solar cells.¹²⁷ In the first Schottky CQD solar cells, light entered through a transparent ohmic contact, and was absorbed by the active CQD film. The back electrical contact was a reflective metal whose work function was selected such that it formed a rectifying junction with the CQD film. Employing active materials such as PbS and PbSe CQDs, typically p-type, required a shallow work function metal such as Mg or Al to create a Schottky barrier.

Following the initial 2007 report of a device employing a PbS CQD/Mg interface as the charge separating junction of a CQD solar cell,¹²⁸ many other reports of CQD Schottky-barrier-based devices were reported.^{74,129–134}

The Schottky architecture, in addition to its functional simplicity and ease of fabrication, proved an excellent architecture for isolating characteristics of the CQD film itself. One 2008 report used the Schottky structure to correlate the size-tuned band positions of the CQD film with the known work functions of various metals (Figure 7a,b) and further quantified the equilibrium free carrier density within the CQD film through Mott–Schottky analysis (Figure 7c).¹³¹

Remarkably, the simple Schottky structure has been optimized to give $\eta > 4.5\%$ through appropriate selection of CQD size.¹³⁴ Unfortunately, Schottky barriers impose a low upper bound on the built-in voltage and thus the V_{OC} .⁹ For this reason, Schottky devices show much lower open-circuit voltages than their bandgap alone would predict from theory.²⁰ Figure 7d shows the J – V characteristic for the highest performing Schottky CQD solar cell with a V_{OC} of 0.47 V for an active CQD layer with a 1.6 eV bandgap.

5. DEPLETED HETEROJUNCTION CQD SOLAR CELLS

Two key limitations in the Schottky CQD solar cell remained to be fully addressed. The first, Fermi level pinning at the Schottky junction, imposes an upper bound on the built-in voltage, and hence V_{OC} , as a result of excessive electronic trap states that arise due to the imperfectly passivated interface between the semiconductor and metal.³⁷ The second limitation was illumination from the nonrectifying side of the device, which ensures that the maximum in the optical generation rate occurs in a region of subunity internal quantum efficiency. Meanwhile, active materials loading challenges in CQD-SSCs limit light absorption, requiring ever thicker porous electrodes while ignoring the possibility of transport through the quantum dots themselves.

The depleted heterojunction (DH)¹⁵ colloidal quantum dot solar cell was developed in an effort to bring together the benefits of the Schottky and QD-SSC architectures. Figure 8 illustrates the physical and energy band structure of the DH device. It employs as its front transparent electrode fluorine-doped tin oxide (FTO) or ITO on glass. Onto the TCO is deposited a layer of (typically) TiO_2 or ZnO , although other wide bandgap semiconductors could be used. While this has typically been nanoporous as in the case of DSSCs, the DH architecture does not demand it, and indeed dense, planar films were used without compromising performance.¹⁰³ On top of this layer is processed a CQD active layer having a thickness of 50–300 nm. A back reflector is finally applied using a deep work function metal such as gold, or a heavily doped oxide such as MoO_3 paired with a reflective metal such as silver.

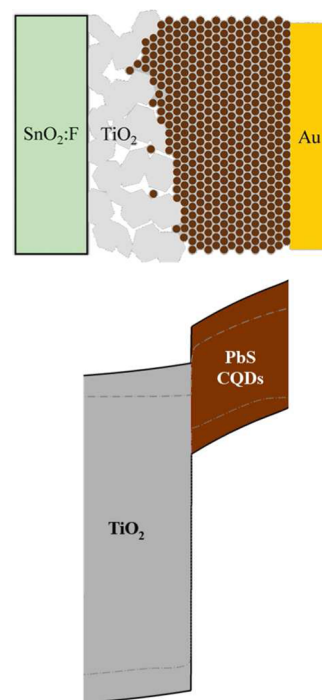


Figure 8. (Top) Structural illustration and (bottom) schematic energy band diagram at short-circuit of depleted heterojunction CQD solar cells. Reprinted with permission from ref 15. Copyright 2010 American Chemical Society.

The DH architecture has rapidly shown promise as an effective architecture for extracting photogenerated current from a CQD film. Through solid-state ligand exchanges to short ligands such as 1-mercaptopropionic acid (MPA),^{15,44,103} 1,2-ethanedithiol (EDT),^{38,135,136} 1,3- and 1,4-benzenedithiol (BDT),^{137,138} formic acid (FA),¹³⁹ as well as to atomic ligands,⁹³ currents have exceeded 21 mA/cm².⁴⁴ The impact of ligand selection, specifically ligand length, has been explored in the context of exciton dissociation⁴⁰ and film conductivity⁴⁸ as illustrated in Figure 9.

The band structure of CQD films as a function of the constituent CQD diameters has been determined through electrochemical¹⁴⁰ and optoelectronic methods.¹⁴¹ These reports suggest that some sizes of CQDs, namely larger ones, would have trouble injecting into TiO_2 due to a reduction of the conduction band offsets as CQD bandgaps become smaller. Figure 10a illustrates how the energy bands of several different PbS CQD sizes line up relative to TiO_2 .

Using the modeling tool SCAPS 3.0.00,¹⁴² a self-consistent one-dimensional electro-optical model was employed to determine the band diagrams (at equilibrium) of three depleted heterojunction devices employing 1.3, 1.1, and 0.9 eV PbS CQDs (Figure 10b). As would be expected from Anderson's rule,¹⁴³ these band diagrams illustrate that at least to a minimum CQD bandgap of 0.9 eV there exists no barrier to electron injection from PbS CQDs to TiO_2 .

The importance of band offsets between the CQD film and TiO_2 film was further explored by adding impurities to a sol-gel-derived TiO_2 electron acceptor.¹⁰³ By simultaneously varying the electron affinity of TiO_2 along with the bandgap of PbS CQDs, the impact of band offsets became evident (Figure 11). Specifically, as the device was biased toward the maximum power point, the electric field within the device was

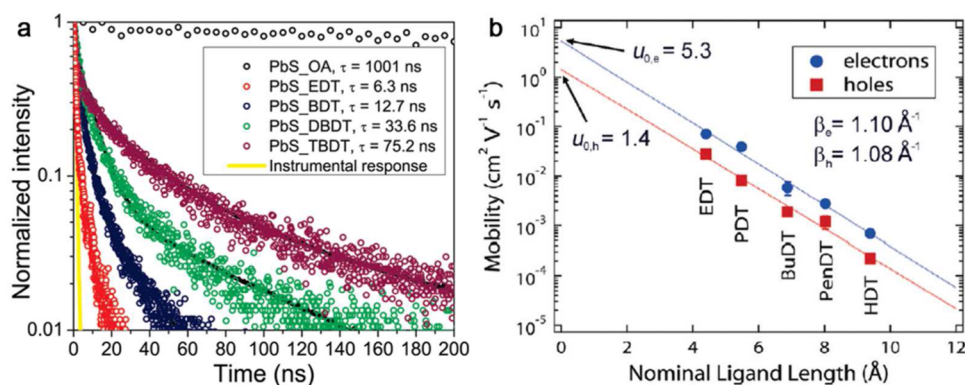


Figure 9. (a) Photoluminescence decay of PbS films passivated with oleic acid (OA), EDT, BDT, 4,4'-dibenzeneedithol (DBDT), and 4,4'-tribenzeneedithol (TBDT) confirming exciton dissociation is faster in short-ligand-passivated CQD films. Reprinted with permission from ref 40. Copyright 2010 American Chemical Society. (b) Electron and hole mobility as a function of ligand length for PbSe CQD films passivated with double-ended thiols including EDT, propanedithiol (PDT), butanedithiol (BuDT), pentanedithiol (PenDT), and hexanedithiol (HDT) demonstrating a linear relationship as measured by field-effect transistors (FETs). Reprinted with permission from ref 48. Copyright 2010 American Chemical Society.

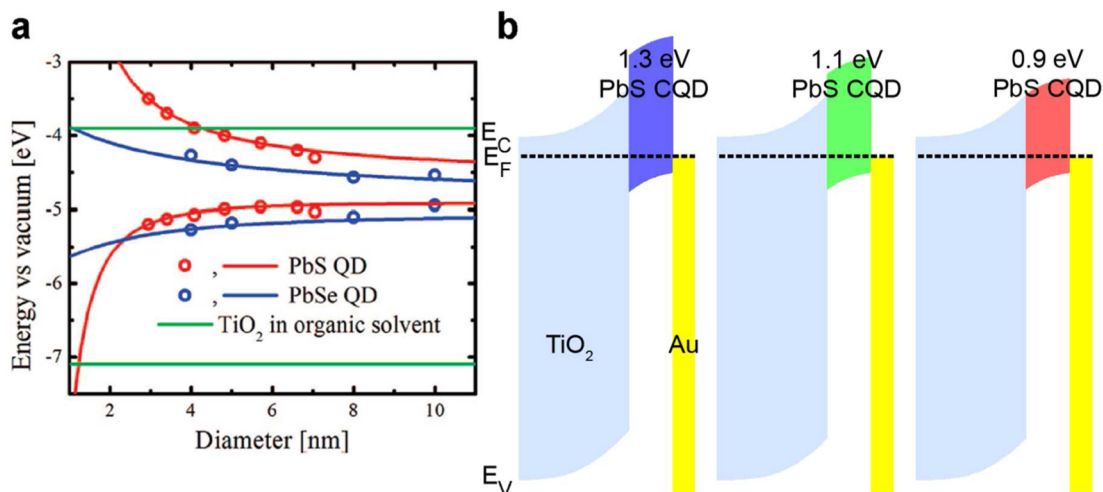


Figure 10. (a) Size-dependent electron affinities (upper three curves) of PbS CQDs (red), PbSe CQDs (blue), and bulk TiO₂ (green). Also shown are the valence band positions of the same three materials (lower three curves). Reprinted with permission from ref 140. Copyright 2008 American Chemical Society. (b) Equilibrium electron band diagrams of TiO₂/PbS/Au depleted heterojunction structures for three different sizes of CQDs as determined from part a. Adapted with permission from ref 15. Copyright 2010 American Chemical Society.

reduced, thereby lowering the drift current collected. In other words, band offsets can facilitate efficient charge extraction in the absence of a strong electric field.

Not surprisingly, a small (or even negative) conduction band offset (red and green bars in Figure 11) maximizes V_{OC} , whereas a negative conduction band offset (red bar) reduces J_{SC} . The optimal conduction band interfacial condition led to a maximized product of V_{OC} , J_{SC} , and FF. It should be noted that this required the use of electron acceptors of different electron affinity to pair optimally with differently size-tuned CQD films (i.e., zirconium-doped TiO₂ for 1.3 eV PbS CQDs and antimony-doped TiO₂ for 1.0 eV PbS CQDs).¹⁰³

Equations 4 and 5 make clear that the depletion width on the CQD side of a semiconductor/CQD junction depends on the relative free carrier densities of each material. More specifically, a junction made up of PbS CQDs ($p = 2 \times 10^{16} \text{ cm}^{-3}$, $\epsilon_{CQD} = 43 \pm 4$)¹⁵ and a wide-bandgap electron acceptor such as TiO₂ ($n = 1 \times 10^{16} \text{ cm}^{-3}$, $\epsilon_{TiO_2} = 55 \pm 10$)¹⁴⁴⁻¹⁴⁷ would have depletion dimensions of $W_{TiO_2} \sim 470 \text{ nm}$ and $W_{CQD} \sim 240 \text{ nm}$ under short-circuit conditions. The implication is that a thinner TiO₂

layer would be incapable of fully depleting a PbS CQD layer even at zero bias, let alone at the maximum power point.

Engineering the deposition conditions for the back contact of the device was also found to be critically important. Dead zones, regions of near-zero IQE, were seen to exist even in devices that were fully depleted under short-circuit conditions.¹⁴⁸ These were remedied by improved thermal evaporation of the metal that was suspected to damage the film. Strategies to improve the back contact have resulted in increased stability and improved performance. MoO₃ has been used as a degenerately doped deep work function contact that both aids in hole extraction through a back surface field¹⁴⁹ and protects the CQD film from subsequent metal deposition (Figure 12).^{135,150} LiF has also been used to protect the CQD film from metals, such as Ni, capable of forming compounds with the constituent CQD elements.¹⁵¹

Short thiols have proved effective at reducing recombination in some CQD films (PbS, CdTe) through improved surface passivation, as evidenced through photoluminescence quantum efficiency measurements,^{84,152} while the same method has

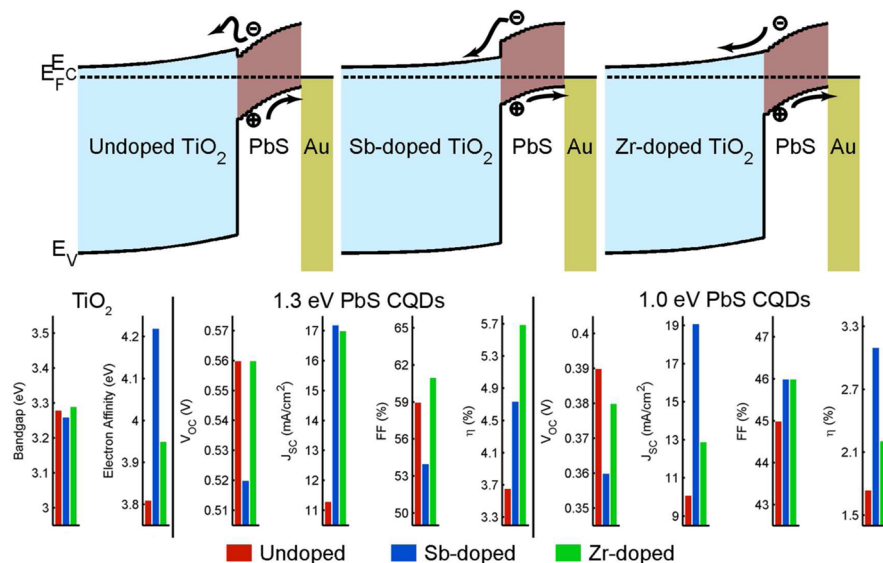


Figure 11. Top row: Depleted heterojunction energy band diagrams using undoped TiO_2 , antimony-doped TiO_2 , and zirconium-doped TiO_2 . Reprinted with permission from ref 103. Copyright 2011 WILEY-VCH Verlag GmbH & Co. KGaA, Weinheim. Bottom row, first and second columns: Bandgap and electron affinity of undoped, Sb-doped and Zr-doped sol-gel TiO_2 . Bottom row, third to sixth columns: Performance metrics of 1.3 eV PbS CQD DH solar cells using the undoped, Sb-doped, and Zr-doped sol-gel TiO_2 including V_{OC} , J_{SC} , FF, and η . Bottom row, seventh to tenth columns: Performance metrics of 1.0 eV PbS CQD DH solar cells of same.

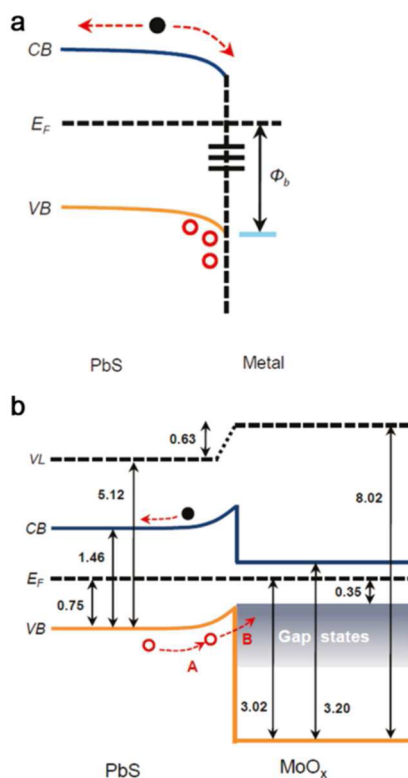


Figure 12. (a) Interfacial defect states generated at metallic back contact. (b) Elimination of defect states in (a) through the use of MoO_3 in place of the metallic back contact. Reprinted with permission from ref 135. Copyright 2011 American Chemical Society.

shown that, in films of other CQD materials (CdSe), short thiols can actually degrade surface passivation.¹⁵² A lowering of the density of deep trap states via atomic ligand passivation was found to further improve current extraction in CQD solar cells.⁹³ A recent study has shown that a combination of atomic ligand passivation and organic thiol passivation reduces trap

states even further.⁴⁴ Figure 13a illustrates how atomic ligands access the hard-to-reach trenches on the CQD surfaces while thiols passivate the rest of the surface. The impact of the enhanced passivation can be seen in Figure 13b. This final hybrid approach leads to improved CQD photovoltaic performance with enhancements in both J_{SC} and V_{OC} relative to previous records, yielding an externally certified power conversion efficiency of 7.0%.⁴⁴

The simplicity of the DH architecture makes it an excellent platform for testing the impact of factors external to the oxide/CQD junction or the quality of the CQD film itself. Recently, plasmonic¹⁵³ and geometric¹⁵⁴ enhancements have been shown to effectively increase photovoltaic performance via enhanced absorption and thus current generation (Figure 14a,b, respectively). In addition, the electrical characteristics of the TCO have been shown to be useful as a remote dopant to the oxide, thus enhancing the built-in field around the junction (Figure 14c).¹⁵⁵

6. CQD SOLAR CELLS USING QUANTUM FUNNELS

Through bandgap engineering, crystalline semiconductors have employed back surface fields.^{149,156} Organic light-emitting diodes¹⁵⁷ and organic solar cells^{158,159} have employed charge transport/blocking layers. A subset of bandgap engineering, bandgap grading, was proposed as a mechanism to further improve PV performance in a variety of materials.^{160–164} Resonant energy transfer between absorbers in organic and dye-sensitized solar cells have helped improve current collection,^{165–167} while compound semiconductors have tuned stoichiometry to generate a favorable electronic band configuration.¹⁶⁸

Figure 10a illustrates the relationship between PbS and PbSe band edges and diameter graphically.^{140,141} One of the more interesting features of this graph is the relative variation in conduction band position versus valence band position in the 3–5 nm range. This range translates into the broad optimal efficiency bandgap peak as predicted in the Shockley–Queisser

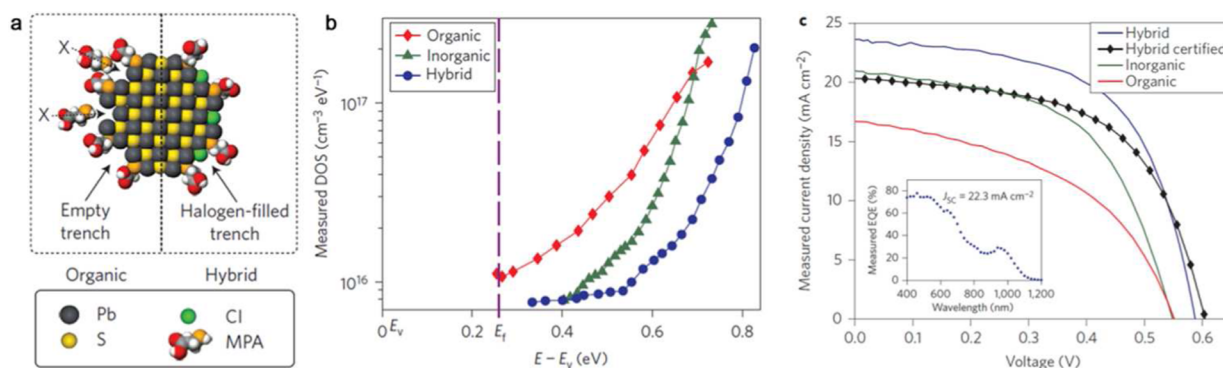


Figure 13. (a) Schematic representation of thiol-passivated CQD surface (left) and hybrid halogen/thiol passivated CQD surface (right). (b) Density of states within the bandgap for organic-, inorganic-, and hybrid-passivated CQD films as measured using the photovoltage transient technique. (c) J - V curves with various passivation strategies. Inset shows EQE of hybrid passivated devices. Reprinted by permission from Macmillan Publishers Ltd.: *Nature Nanotechnology* (ref 44), copyright 2012.

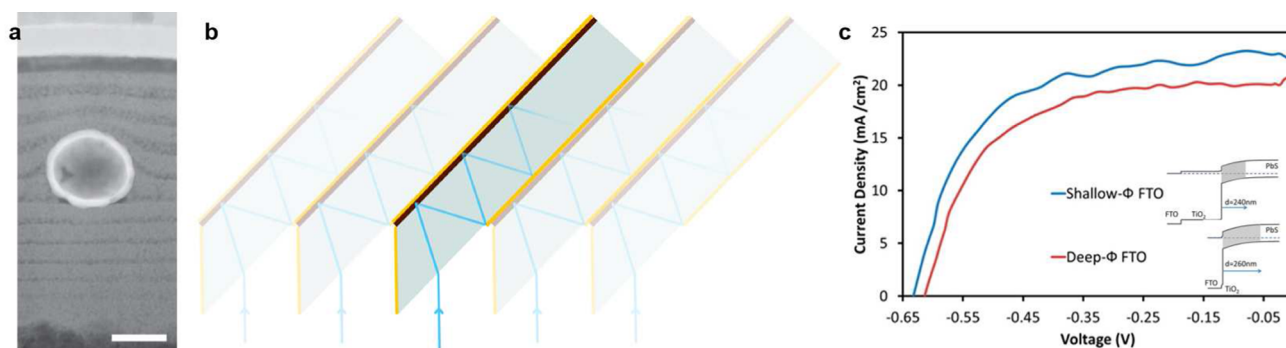


Figure 14. (a) Cross-section of depleted heterojunction employing plasmonic nanoshells for improved absorption. Scale bar, 100 nm. Reprinted with permission from ref 153. Copyright 2013 American Chemical Society. (b) Scheme for periodic arrangement of depleted heterojunction solar cells employing a folded-light-path configuration to allow for multiple passes. Reprinted by permission from Macmillan Publishers Ltd.: *Scientific Reports* (ref 154), copyright 2013. (c) Performance enhancement due to a shallow work function TCO and its impact on optimal TiO₂ thickness and depletion width (inset). Reprinted with permission from ref 155. Copyright 2013 American Chemical Society.

limit.³⁴ Within this range, the conduction band varies by several meV, while the valence band hardly varies at all.

Colloidal assemblies of CQDs, suspended in solution, have demonstrated, through liquid-phase luminescence studies that all exciton energy couples to the smallest bandgap within the assembly.¹⁶⁹ Exciton funneling has also been shown in CQD solids where luminescence primarily occurs at the smallest bandgap in an array of different CQD sizes stacked on top of one another in coupled CQD films.^{97–99} This funneling concept was applied to the back of a DH PbS CQD solar cell in order to aid in current collection under operating conditions (i.e., at the maximum power point) when the CQD film was not fully depleted (Figure 15).¹⁰⁰

Note that the simulated results from Figure 15b place the optimal grading depth well within the depletion region (at short-circuit conditions). In other words, in order to take advantage of a quantum funnel, it needs to be placed within the short-circuit depletion region rather than at its edge. One might expect that this surprising result would not, therefore, lead to an enhancement in device current (i.e., J_{SC}), but instead in fill factor. Further conceptual justification for this nuance is explained in detail in Figure 16.

Figure 16 provides a conceptual framework justifying FF improvement without an appreciable increase in J_{SC} . The top left schematic shows a typical depleted heterojunction CQD solar cell that is fully depleted under short-circuit conditions. At the maximum power point (bottom left schematic), the band

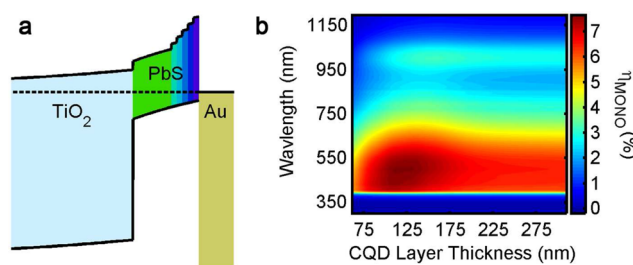


Figure 15. (a) Band diagram of a quantum funnel device and (b) simulated monochromatic power conversion efficiency for a device employing an optimally placed quantum funnel. For thick devices, spectral performance is capped by carrier extraction, while for devices with optimally placed quantum funnels, performance increases over all wavelengths. Adapted with permission from ref 100. Copyright 2011 American Chemical Society.

bending is reduced in the active material, and a quasineutral region near the back contact begins to grow. Once the quasineutral region is longer than the diffusion length of electrons, extracted current is reduced, and recombination within the quasineutral region increases. By appending a quantum funnel onto the back of the standard DH device (top middle schematic), extracted current under short-circuit conditions is unaffected; in fact, it may even grow if the quantum funnel absorbs a significant amount of light. Unfortunately, when this structure moves toward the maximum

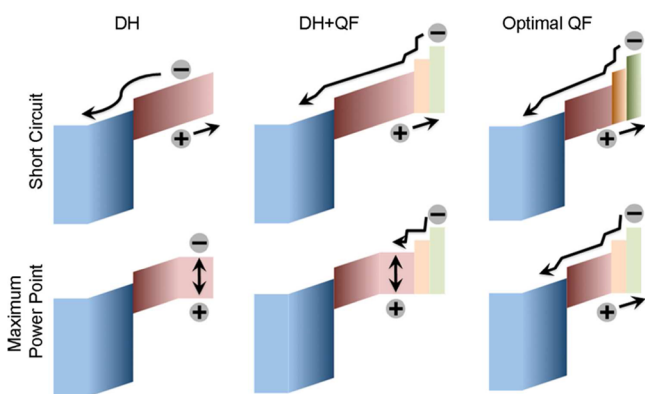


Figure 16. Spatial band diagrams of a DH CQD solar cell (left column), a DH CQD solar cell with an appended quantum funnel (middle column), and a slightly truncated DH CQD solar cell with an appended quantum funnel (right column) at short-circuit (top row) and maximum power point conditions (bottom row).

power point (bottom middle schematic) and the bands begin to unbend, all the electrons that were successfully funneled into the smallest bandgap material will be faced with a large quasineutral region they are unable to traverse. In this case, despite successful funneling, no gain in extracted current at the maximum power point will be observed, and overall efficiency remains unchanged relative to the standard DH device. If, instead of using the standard DH device, we apply the quantum funnel to a truncated DH cell, an electric field persists throughout the device both at short-circuit (top right schematic) and at maximum power point (bottom right schematic) conditions. This architecture would not be expected to result in any J_{SC} enhancements, but would be expected to extract additional current at the maximum power point as compared to the other two structures. Experimental results confirmed that the fill factor was the primary beneficiary of an optimally placed quantum funnel.¹⁰⁰

7. DEPLETED BULK HETEROJUNCTION CQD SOLAR CELLS

As described in sections 5 and 6, collecting photogenerated minority carriers (electrons) from the CQD film is critical to improving performance. The quantum funnel¹⁰⁰ described a way to manipulate the energetic landscape of the CQD film to aid in carrier extraction. The organic PV community, on the other hand, found that, by manipulating the geometric landscape of the p–n interface, it could ensure that any photogenerated exciton was no more than one exciton diffusion length away from the charge separating interface. This three-dimensional interpenetrating interface is known as the organic donor–acceptor bulk heterojunction.²³

Unlike in organic PV, the DH CQD device is capable of collecting carriers generated within the depletion region of the device. This caps the total device thickness to the thickness of the depletion region (plus one diffusion length of electrons in the CQD film, ~ 10 nm¹⁶). The implementation of a bulk heterojunction structure extended the depletion region deeper into the device, facilitating the use of thicker, more absorbing CQD layers.^{92,170,171}

Figure 17a,b¹⁷¹ depicts a planar DH and textured depleted bulk heterojunction (DBH) device. Here the pink regions represent depleted portions of the CQD film, while red regions are quasineutral. Because the DBH structure pushes the built-in

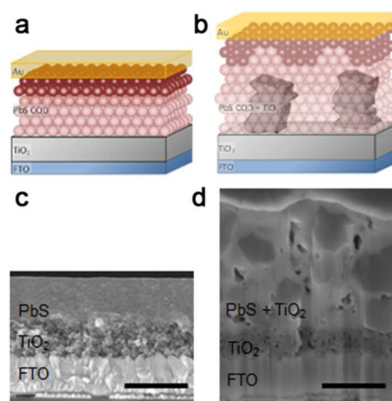


Figure 17. Schematics of a (a) planar DH device and a (b) textured DBH device. (c,d) Cross sectional SEMs of devices of same. In each case the scale bar is 500 nm. Reprinted with permission from ref 171. Copyright 2011 WILEY-VCH Verlag GmbH & Co. KGaA, Weinheim.

electric field deeper within the device, thicker films can be built up, and therefore, longer, less strongly absorbed wavelengths are more readily converted into extracted current.

The DBH electron acceptor has been built using presynthesized large TiO_2 nanoparticles, through lithographically defined nanopillars (Figure 18)¹⁷² or using bottom-up grown nanowires.^{170,173,174} In all cases, PbS CQDs were infiltrated into the large voids of the electron acceptor matrix, forming the bicontinuous bulk heterojunction.

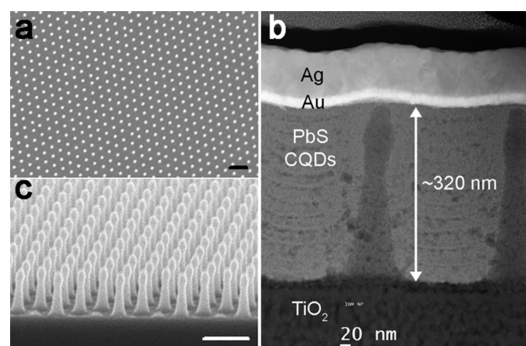


Figure 18. (a, b) Bare TiO_2 nanopillar substrates. Scale bars are 500 nm. (c) Cross sectional SEMs of PbS CQD-infiltrated nanopillar DBH device. Reprinted with permission from ref 92. Copyright 2012 WILEY-VCH Verlag GmbH & Co. KGaA, Weinheim.

The DBH architecture allowed for both enhanced absorption through increased CQD film thickness (Figure 19a) and increased IQE through reduction of Shockley–Reed–Hall (SRH) recombination in the vicinity of the bulk heterojunction interface (Figure 19b). These findings are in good agreement with previously analyzed nanopillar solar cells.¹⁷⁵ Low hysteresis in the illuminated J – V curves of DBH samples⁹² (compared with planar DH samples) confirms that, in the bulk heterojunction structure, carrier collection wins over carrier trapping.^{176,177}

DBH devices are more susceptible to bimolecular recombination than planar DH devices due to an increased interfacial area. Conduction band offsets therefore become more critical in such structures, wherein an electron injected from the CQD phase into the TiO_2 phase must be prevented from back-recombining over the course of its long, narrow path to the

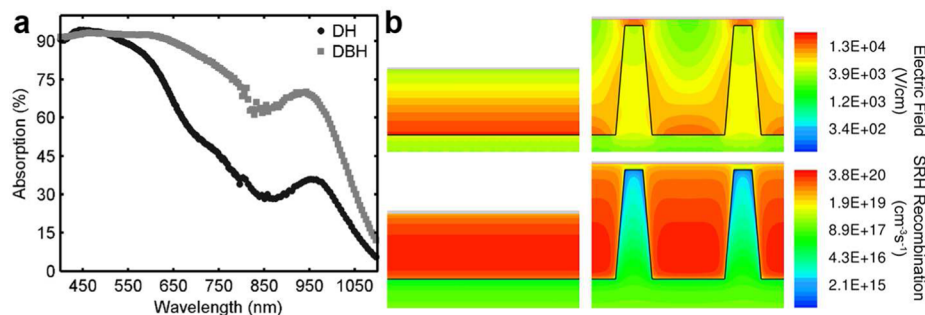


Figure 19. (a) DH and DBH device absorption characteristics. Reprinted with permission from ref 171. Copyright 2011 WILEY-VCH Verlag GmbH & Co. KGaA, Weinheim. (b) Two-dimensional device simulation illustrating enhanced electric field and reduced Shockley–Read–Hall recombination in the volumetric vicinity of the TiO₂ electron acceptor. All simulations are at the maximum power point. Reprinted with permission from ref 92. Copyright 2012 WILEY-VCH Verlag GmbH & Co. KGaA, Weinheim.

cathode. This condition imposes a slight penalty on built-in voltage for DBH devices compared to their planar DH counterparts.

8. BULK–NANO HETEROJUNCTION CQD SOLAR CELLS

All device architectures to this point have relied on transparent in-coupling of light into the active layer. Several reports, however, use CQDs as the primary absorber, but additionally use other active materials to achieve high performance.

One of the first reported devices utilizing colloidal quantum dots in a solar cell employed nanocrystals of CdTe and CdSe.⁷⁷ Here the CdTe nanocrystals exhibited bulk-like optoelectronic characteristics (i.e., they were not quantum confined), while quantum-confined CdSe CQDs were used to augment absorption. The resultant planar stack was a bulk–nano heterojunction (BNH).

Recently, a planar BNH device employing a colloidal Bi₂S₃ nanocrystal¹⁷⁸ film as the n-type layer and PbS CQDs as the p-type layer¹⁷⁹ was made interpenetrating through a solution-phase mixture of the two moieties.¹⁸⁰ The resultant device exhibited current collection from both the Bi₂S₃ and size-tuned PbS phases. This was achieved by allowing photogenerated carriers in both materials to be in the vicinity of a charge separating junction, similar to organic PV bulk heterojunctions.²³ Figure 20 illustrates the interpenetrating p- and n-type materials.

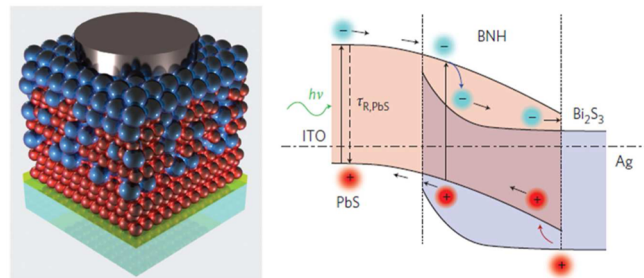


Figure 20. (Left) Illustration of a BNH device wherein the red spheres represent the p-type quantum dots and the blue spheres represent the n-type nanoparticles. Substrate, TCO, and metal electrode are also shown for reference. (right) Schematic band diagram of BNH with interpenetrating p-type and n-type layers. The p-type and n-type bands are drawn overlapping to accentuate the geometric relationship between the interpenetrating phases. Reprinted by permission from Macmillan Publishers Ltd.: *Nature Photonics* (ref 180), copyright 2012.

Other reports use infrared-absorbing CQDs to augment already functional solar cells using more conventional materials incapable of absorbing much beyond the visible or near-IR.^{181–183}

9. QUANTUM JUNCTION SOLAR CELLS

While the DH and BNH address many of the limitations of earlier architectures, they continue to surrender available open-circuit voltage, even if both the CQDs and electron acceptors were degenerately doped, a condition that could have other deleterious impacts, such as the unintended creation of a tunnel junction or the reduction of depletion width, thus limiting drift current collection.³⁷ At a minimum they require re-engineering of the electron acceptor when the CQD absorber is size-tuned to a different bandgap.¹⁰³

This challenge was recently overcome by employing size-tuned CQDs on each side of the rectifying junction. This required the development of both n-type and p-type films within a CQD stoichiometry.

CQD doping has been demonstrated primarily through incorporation of dopant impurities onto the CQD surfaces^{184,185} or into the CQD crystal lattice.^{185–189} Doping has also been demonstrated by exposing CQD films to various atmospheres, solvents, or redox couples.^{67,75,190,191}

Ligands are one further critical factor in the net doping of a CQD film.^{133,191,192} In 2012, it was reported that PbS CQD films could be manipulated to be both n-type and p-type through selection of surface ligands and exposure (or lack thereof) to air.¹⁹³ Figure 21a illustrates how the doping of PbS CQD films can vary with ligand.

Developing n-type CQD films¹⁹⁵ opened the door to p–n junction-like structures wherein both sides of the junction could be size-tuned to achieve the same or different bandgaps as desired. This device, known as the quantum junction (QJ), removed the band offset challenge of DH and BNH structures.¹⁹⁴ Figure 21b shows the turn-on behavior of quantum junctions as a function of differently size-tuned PbS CQDs for the n-type and p-type layers.

Figure 22a illustrates how the current for small-bandgap DH devices is blocked while it can be collected for QJ devices. The linear relationship between CQD bandgap and V_{OC} can be seen in Figure 22b.

Further optimizations of the device electrode,⁴⁵ PbS doping,⁴⁵ and PbS passivation¹⁹⁶ recently led to solar power conversion efficiencies η of 6.6%.

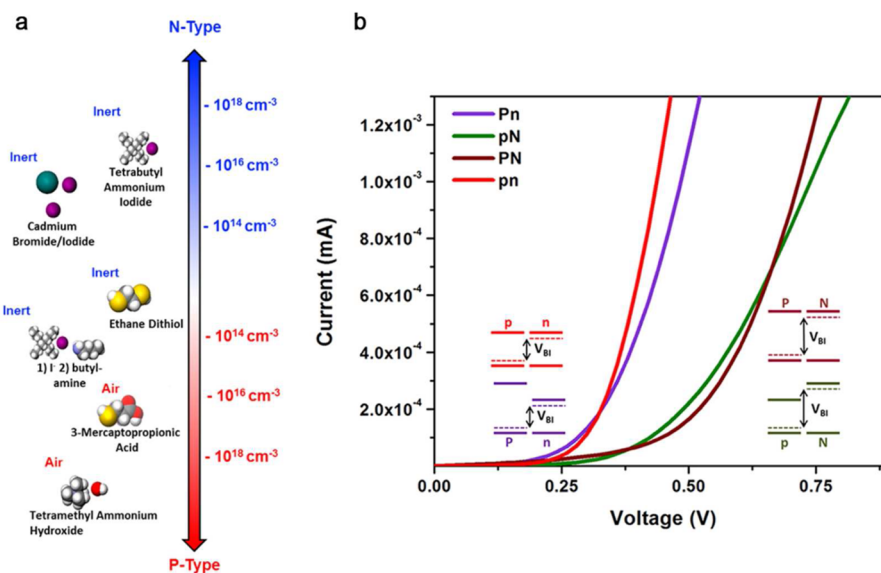


Figure 21. (a) Doping density as a function of atmosphere and ligand for PbS CQD films. Reprinted with permission from ref 193. Copyright 2012 American Chemical Society. (b) Turn-on characteristic of quantum junctions with different size-tuned n-type and p-type PbS CQDs. Reprinted with permission from ref 194. Copyright 2012 American Chemical Society.

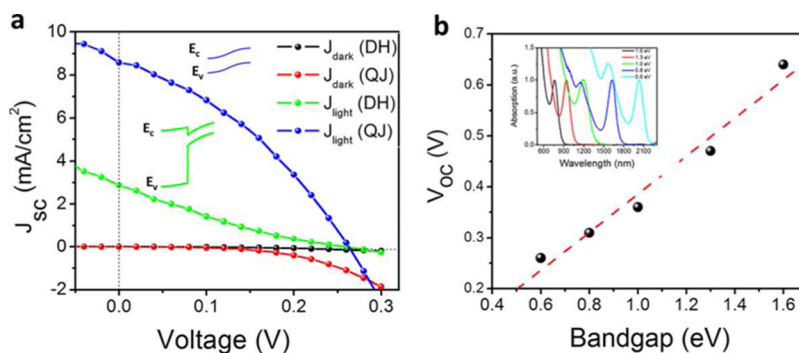


Figure 22. (a) J - V characteristics of DH and QJ devices for 0.6 eV PbS CQDs. (b) V_{OC} as a function of CQD bandgap exhibiting linear trend for a QJ structure. Reprinted with permission from ref 194. Copyright 2012 American Chemical Society.

A new variant on the quantum junction, an analogue to p-i-n structures used in amorphous silicon solar cells,¹⁰ employing a p⁺-n-n⁺ graded doping structure further enhanced device performance to 7.4%.¹⁹⁷

The potential of the quantum junction architecture can most clearly be seen in the context of multiple junction solar cells. Whereas heterojunction devices would require careful engineering of electron acceptor materials for the smallest bandgap junctions, the quantum junction avoids this problem entirely by employing both n-type and p-type phases of the same size CQDs.

10. MULTIPLE-JUNCTION CQD SOLAR CELLS

All the architectures discussed to this point focus on approaching as closely as possible the single-junction Shockley-Queisser limit of $\eta = 31\%$.³⁴ Colloidal quantum dots, however, allow for facile tuning of the bandgap, thereby making them ideal candidates for multiple junction solar cells.

By optimally selecting the constituent bandgaps, multiple junctions can be stacked and connected through ideal recombination layers in order to exceed the single-junction Shockley-Queisser limit.²⁰ Figure 23a shows the graphical calculation of the ideal single junction solar cell efficiency and

further applies the same concepts to multiple junction solar cells (Figure 23b).

The optimal tandem (also known as double junction) active material bandgaps are 1.6 and 1.0 eV for the first and second junctions, respectively. The first cell absorbs all photons with energy greater than 1.6 eV. The second cell absorbs all photons with energy between 1.0 and 1.6 eV. Figure 24 illustrates how the photogenerated electrons from the first cell, J1, recombine with the photogenerated holes from the second cell, J2 (or vice versa depending on the configuration of the cells), in a recombination layer, RL. The ideal recombination layer is transparent to all wavelengths absorbed by J2 and allows all electrons from J1 to recombine with all of the holes from J2 without any losses. As these two cells are in series, a current matching condition is imposed. For optimal efficiency, the current generated in J1 and J2 should be equal and can be controlled by adjusting absorption or extraction characteristics in each. The output current, therefore, in a tandem cell is equal to the current of each constituent cell, while the output voltage is the sum of the voltages of each constituent cell.

Two reports of CQD tandem cells appeared in mid-2011,^{198,199} both demonstrating the principle of voltage addition in tandem devices.

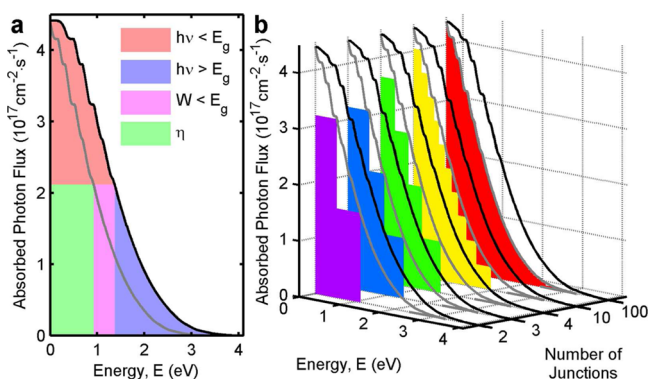


Figure 23. Limiting efficiencies of solar cells for (a) single junction solar cells and their application to (b) multiple junction solar cells. In all cases, the black curves represent the total number of photons an opaque active material of energy E could absorb (i.e., all photons with energy greater than E), and gray curves represent the maximum work that can be extracted for each of those materials of energy E . The ratio of the area in green in (a) to the area under the black curve is the device efficiency. Note that, for multiple junction solar cells, the maximum efficiency can exceed any solar cells composed of fewer junctions. Reprinted with permission from ref 20. Copyright 1980 American Institute of Physics.

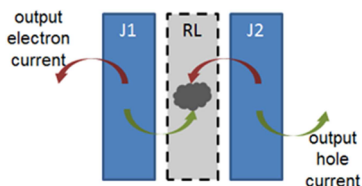


Figure 24. Tandem configuration illustrating recombination between hole current from the first junction (J1) with electron current from the second junction (J2).

The first report employed inverted depleted heterojunctions with gold islands serving as the recombination layer,¹⁹⁸ whereas the second report employed depleted heterojunction cells with a graded recombination layer.¹⁹⁹ Figure 25a demonstrates the principle of current matching and voltage addition in optimally designed tandem cells. Highlighted in Figure 25b is the contribution of each junction to the overall current generated.

The graded recombination layer facilitates efficient electron–hole recombination between the two junctions thereby satisfying the current matching condition.²⁰⁰ Meanwhile, optimization of each constituent cell^{201,202} is also crucial to achieving the overall single junction to double junction efficiency enhancement predicted by theory.²⁰

11. HOT-CARRIER EFFECTS IN CQD MATERIALS: DEVICE IMPLICATIONS

When photons with energy greater than the bandgap are absorbed, they generate excitons whose energy is also greater than the bandgap. These hot excitons typically relax very quickly to the band edge through phonon emission, losing their energy in excess of the fundamental excitonic level. While this relaxation time is typically very fast, it is much slower in CQDs than in bulk solids due to the relative scarcity of available states.^{8,203–205} CQDs also offer the promise of entering the hot-photon bottleneck regime^{206,207} at solar intensities without the use of a concentrator.^{8,208,209} Taking advantage of these hot excitons to exceed the Shockley–Queisser limit³⁴ within the

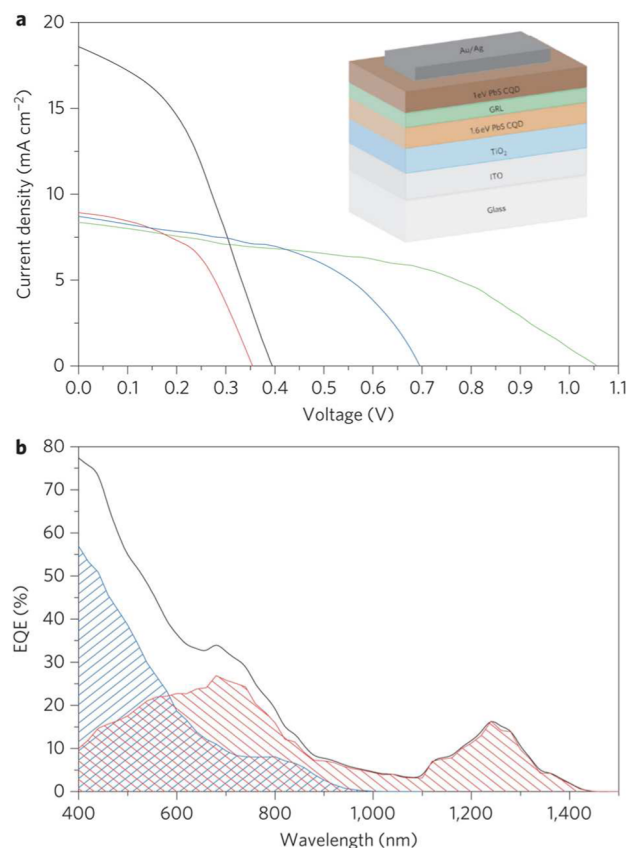


Figure 25. (a) J – V of the large-bandgap (blue), small-bandgap (black), and tandem (green) cells under AM 1.5 G illumination. Also shown is the small-bandgap cell when filtered by a large-bandgap cell. (Inset) Structural cross-section of the tandem cell showing the 1.6 eV CQD first cell, recombination layer, and 1.0 eV CQD second cell. (b) EQE performance of each junction and the overall tandem device. Reprinted by permission from Macmillan Publishers Ltd.: *Nature Photonics* (ref 199), copyright 2011.

constraints of a single-junction solar cell can take two forms: hot electron transfer and multiple exciton generation.

11.1. Hot-Electron Transfer

Theory dictates that solar cells capable of extracting hot carriers can in principle exceed the single-junction Shockley–Queisser limit.^{210,211} Extracting hot carriers directly presents a significant challenge due to fast relaxation from the excited state to the band edge.²¹² The ideal hot-electron structure involves all hot electrons converging to one excited state energy level that aligns with the work function of a selective contact. In this configuration, hot electrons warm up band edge electrons, and, in principle, no energy is lost due to phonons.^{212,213} Figure 26 shows a possible n–i–p implementation of a hot-carrier solar cell where tunnel junctions are used as selective contacts.²¹⁴

The ultimate architecture notwithstanding, the most important obstacle to overcome in realizing hot-carrier extraction is increasing the hot-carrier lifetime. It has been demonstrated in PbSe CQDs that one carrier can sacrifice its excited state energy to promote a longer excited state lifetime in the complementary carrier.²¹⁵ This slow cooling of excited states was further demonstrated to ~ 20 ps through core–shell CQD structures.²¹⁶ Indeed this same structure showed that the hot electron tunneled to the shell and could be extracted before relaxing to the band edge. A 2010 report demonstrated that hot electrons could be extracted into a titania electron acceptor,²¹⁷

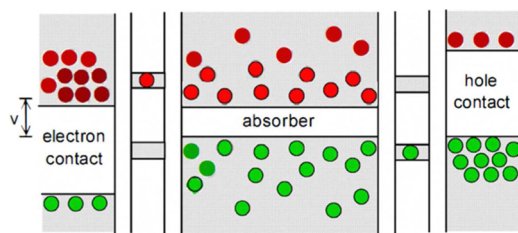


Figure 26. Conceptual n–i–p implementation of a hot carrier solar cell. Reprinted with permission from ref 214. Copyright 2010 Institute of Electrical and Electronics Engineers.

a remarkable achievement since cold, band edge electrons could also be injected into the titania within this system.²¹⁸ This report hints at the possibility of a viable path to such structures employing PbSe CQDs.

11.2. Multiple Exciton Generation

Multiple exciton generation (MEG) and extraction has been studied in bulk materials^{219,220} and has recently been of much interest in the CQD community.^{8,203–205,221–223} In ideal MEG solar cells, excitons whose energy is well above twice the bandgap will decay to the bandgap energy and produce extra electron–hole pairs. If these extra excitons can be collected prior to rapid recombination mechanisms such as Auger recombination,^{224–233} again the single-junction Shockley–Quiesser limit³⁴ can be overcome. Along these lines, developing methods to observe hot exciton cooling has become of paramount importance. Many of these techniques have been developed, either for CQD films in particular, or previously for other materials systems, but some of the results have led to conflicting conclusions surrounding whether or not MEG is enhanced in CQD films versus their bulk counterparts.^{55,234–250}

A past problem now resolved was the overestimation of quantum yield due to photocharging of quantum dots.²⁵¹

Figure 27 illustrates the MEG quantum yield for different MEG efficiencies with the expected efficiency enhancement.²⁵²

A 2010 report²²² demonstrating IQE over 100% was followed by a 2011 report²²³ demonstrating EQE of over 100%, both within photovoltaic devices, emphatically demonstrating useful MEG (Figure 28). Prior reports had limited the observation of MEG to structures specifically designed for

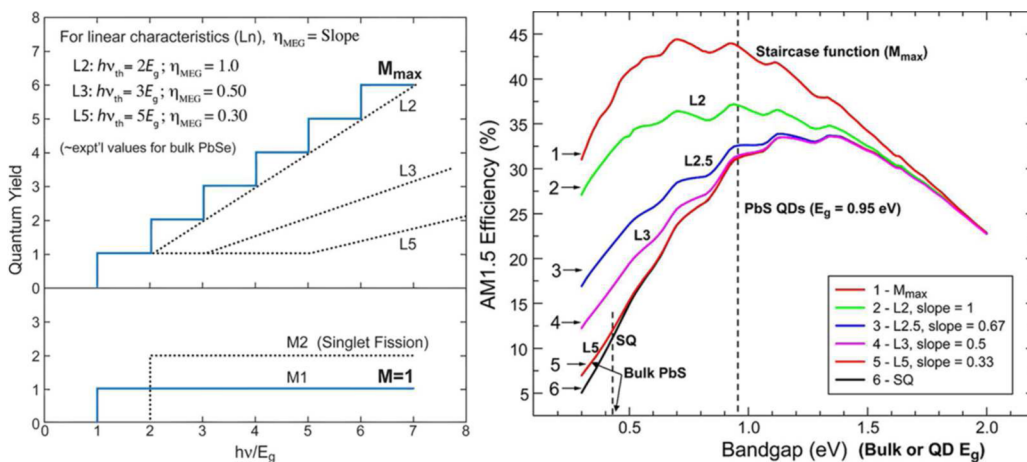


Figure 27. Quantum yield (left) and η limit (right) for different MEG efficiencies. Reprinted with permission from ref 252. Copyright 2012 American Chemical Society.

MEG observation/characterization^{253–256} or other, nonphoto-voltaic applications.²⁵⁷

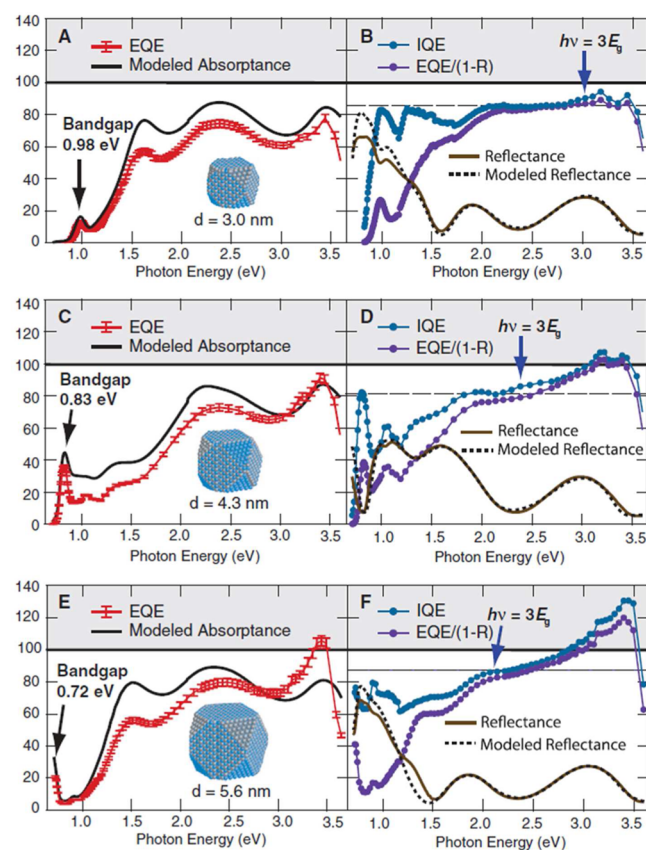


Figure 28. Measured EQE (red curves), modeled absorbance (black curves), IQE (blue curves), reflectance (brown curves), modeled reflectance (dashed black curves), and EQE/(1 – R) (purple curves) illustrating an increase in IQE at $3E_g$. From ref 223. Reprinted with permission from AAAS.

12. CONCLUSIONS

The materials chemistry of CQDs suspended in solution and processed into films has provided a foundation onto which

useful photovoltaic devices can be built. These active materials offer the benefits of solution processing paired with the flexibility of adjustable bandgaps, tailored to suit a particular need.

In parallel with these advances, pursuing device geometries that better leverage the available electronic properties of CQD films has borne fruit in further advancing CQD solar cell performance. Through the architectures discussed here, CQD-based solar cells have achieved over η of over 8.5%. They have also been employed in multijunction architectures and have been deployed to exploit multiple exciton generation. A summary of performance versus device architecture is presented in Table 1.

Table 1. Best Power Conversion Efficiency Achieved by Each Device Architecture Class

architecture	η (%)	ref
CQD-SSC	5.4	27
QD-SSC (SILAR or CBD)	5.6	124
Schottky	4.6	134
depleted heterojunction	8.5	155
quantum funnel	2.7	100
depleted bulk heterojunction	7.3	173
bulk–nano heterojunction	4.9	180
quantum junction	7.4	197
multijunction (tandem)	4.2	199

Further advances in performance will continue to benefit from parallel improvements in CQD materials chemistry, especially the realization of CQD solids that combine high mobility for electrons and holes, and that simultaneously minimize the density of midgap recombination centers. Much remains to be achieved in the materials processing of CQD solids as well to enable dense, and potentially ordered, CQD films that offer a smooth and consistent energy landscape for the flow of charge carriers.

At the same time, the field of CQD PV architecture offers much room for further progress. The bulk heterojunction architecture has yet to be fully mastered: indeed, models suggest that further performance progress will result when structured electrodes are taller, thinner, and more heavily doped, and when an interpenetrating top electrode is deployed to overcome transport limitations of the majority carrier in the CQD film. While tandem CQD solar cells have been built, their further optimization is set to produce further advances in performance over single-junction devices, which will in turn set the stage for quantum-tuned triple-junction and multijunction CQD photovoltaics. Finally, absorption enhancements via photonic in-coupling, plasmonic near-field enhancements, and geometric optics remain fertile ground for improving the absorption of light in thin CQD films by increasing the effective path length of weakly absorbed light within the absorber.

Broadly, the rapid pace of CQD solar cell performance shows no signs of abating, and indeed has much more room, and also an urgent need, to improve further, in view of the ever-growing global hunger for renewable energy solutions that harvest the clean, free, and abundant solar resource reaching the earth's surface.

AUTHOR INFORMATION

Corresponding Author

*E-mail: ted.sargent@utoronto.ca.

Author Contributions

I.J.K. and E.H.S. generated a detailed outline of the manuscript, I.J.K. drafted the full manuscript, and I.J.K. and E.H.S. reviewed and edited to produce the final submission.

Notes

The authors declare no competing financial interest.

Biographies



Illan Kramer received a B.A.Sc. (Electrical Engineering) from the University of Waterloo in 2004 and a M.Eng. from McGill University (Electronics) in 2006. He recently completed a Ph.D. in Professor Edward H. Sargent's group at the University of Toronto. His research focused on developing and optimizing architectures for colloidal quantum dot photovoltaic devices with emphasis on energetic considerations for efficient charge extraction.



Ted Sargent received the B.Sc.Eng. (Engineering Physics) from Queen's University in 1995 and the Ph.D. in Electrical and Computer Engineering (Photonics) from the University of Toronto in 1998. He holds the rank of Professor in the Edward S. Rogers Sr. Department of Electrical and Computer Engineering at the University of Toronto, where he holds the Canada Research Chair in Nanotechnology. He is a Fellow of the AAAS and Fellow of the IEEE.

ACKNOWLEDGMENTS

The authors would like to thank Oleksandr Voznyy for illuminating discussions on transport mechanisms in CQD films. This publication is based in part on work supported by Award KUS-11-009-21, made by King Abdullah University of Science and Technology (KAUST).

ABBREVIATIONS

J_{sc} short-circuit current density

V_{OC}	open-circuit voltage
FF	fill factor
η	power conversion efficiency
EQE	external quantum efficiency
IQE	internal quantum efficiency
DH	depleted heterojunction
DBH	depleted bulk heterojunction
BNH	bulk nano heterojunction
QJ	quantum junction
RL	recombination layer
MEG	multiple exciton generation

REFERENCES

- Donegá, C. de M. *Chem. Soc. Rev.* **2011**, *40*, 1512.
- Konstantatos, G.; Howard, I.; Fischer, A.; Hoogland, S.; Clifford, J.; Klem, E.; Levina, L.; Sargent, E. H. *Nature* **2006**, *442*, 180.
- Clifford, J. P.; Konstantatos, G.; Johnston, K. W.; Hoogland, S.; Levina, L.; Sargent, E. H. *Nat. Nanotechnol.* **2009**, *4*, 40.
- Sun, L.; Choi, J. J.; Stachnik, D.; Bartnik, A. C.; Hyun, B.-R.; Malliaras, G. G.; Hanrath, T.; Wise, F. W. *Nat. Nanotechnol.* **2012**, *7*, 369.
- Colvin, V. L.; Schlamp, M. C.; Alivisatos, A. P. *Nature* **1994**, *370*, 354.
- Tessler, N.; Medvedev, V.; Kazes, M.; Kan, S.; Banin, U. *Science* **2002**, *295*, 1506.
- Talapin, D. V.; Lee, J.-S.; Kovalenko, M. V.; Shevchenko, E. V. *Chem. Rev.* **2009**, *110*, 389.
- Nozik, A. J.; Beard, M. C.; Luther, J. M.; Law, M.; Ellingson, R. J.; Johnson, J. C. *Chem. Rev.* **2010**, *110*, 6873.
- Nelson, J. *The Physics of Solar Cells*; Imperial College Press: London, 2003.
- Carlson, D. E.; Wronski, C. R. *Appl. Phys. Lett.* **1976**, *28*, 671.
- Okamoto, H.; Nitta, Y.; Adachi, T.; Hamakawa, Y. *Surf. Sci.* **1979**, *86*, 486.
- Tawada, Y.; Okamoto, H.; Hamakawa, Y. *Appl. Phys. Lett.* **1981**, *39*, 237.
- Shah, A.; Meier, J.; Vallat-Sauvain, E.; Wyrsh, N.; Kroll, U.; Droz, C.; Graf, U. *Sol. Energy Mater. Sol. Cells* **2003**, *78*, 469.
- G03 Committee. *Tables for Reference Solar Spectral Irradiances: Direct Normal and Hemispherical on 37 Tilted Surface*; ASTM International: West Conshohocken, PA, 2012.
- Pattantyus-Abraham, A. G.; Kramer, I. J.; Barkhouse, A. R.; Wang, X.; Konstantatos, G.; Debnath, R.; Levina, L.; Raabe, L.; Nazeeruddin, M. K.; Grätzel, M.; Sargent, E. H. *ACS Nano* **2010**, *4*, 3374.
- Johnston, K. W.; Pattantyus-Abraham, A. G.; Clifford, J. P.; Myrskog, S. H.; Hoogland, S.; Shukla, H.; Klem, E. J. D.; Levina, L.; Sargent, E. H. *Appl. Phys. Lett.* **2008**, *92*, 122111.
- Zhitomirsky, D.; Voznyy, O.; Hoogland, S.; Sargent, E. H. *ACS Nano* **2013**, *7*, 5282.
- Cademartiri, L.; Montanari, E.; Calestani, G.; Migliori, A.; Guagliardi, A.; Ozin, G. A. *J. Am. Chem. Soc.* **2006**, *128*, 10337.
- Moreels, I.; Lambert, K.; Smeets, D.; De Mynck, D.; Nollet, T.; Martins, J. C.; Vanhaecke, F.; Vantomme, A.; Delerue, C.; Allan, G.; Hens, Z. *ACS Nano* **2009**, *3*, 3023.
- Henry, C. H. *J. Appl. Phys.* **1980**, *51*, 4494.
- Kroon, J. M.; Wienk, M. M.; Verhees, W. J. H.; Hummelen, J. C. *Thin Solid Films* **2002**, *403–404*, 223.
- Snaith, H. J. *Nat. Photonics* **2012**, *6*, 337.
- Shaheen, S. E.; Brabec, C. J.; Sariciftci, N. S.; Padinger, F.; Fromherz, T.; Hummelen, J. C. *Appl. Phys. Lett.* **2001**, *78*, 841.
- O'Regan, B.; Grätzel, M. *Nature* **1991**, *353*, 737.
- Rühle, S.; Shalom, M.; Zaban, A. *ChemPhysChem* **2010**, *11*, 2290.
- Mora-Seró, I.; Giménez, S.; Fabregat-Santiago, F.; Gómez, R.; Shen, Q.; Toyoda, T.; Bisquert, J. *Acc. Chem. Res.* **2009**, *42*, 1848.
- Zhang, H.; Cheng, K.; Hou, Y. M.; Fang, Z.; Pan, Z. X.; Wu, W. J.; Hua, J. L.; Zhong, X. H. *Chem. Commun.* **2012**, *48*, 11235.
- Leventis, H. C.; O'Mahony, F.; Akhtar, J.; Afzaal, M.; O'Brien, P.; Haque, S. A. *J. Am. Chem. Soc.* **2010**, *132*, 2743.
- Ning, Z.; Tian, H.; Yuan, C.; Fu, Y.; Sun, L.; Ågren, H. *Chem.—Eur. J.* **2011**, *17*, 6330.
- Ning, Z.; Yuan, C.; Tian, H.; Fu, Y.; Li, L.; Sun, L.; Ågren, H. *J. Mater. Chem.* **2012**, *22*, 6032.
- Clifford, J. P.; Johnston, K. W.; Levina, L.; Sargent, E. H. *Appl. Phys. Lett.* **2007**, *91*, 253117.
- Kramer, I. J.; Sargent, E. H. *ACS Nano* **2011**, *5*, 8506.
- Etgar, L.; Moehl, T.; Gabriel, S.; Hickey, S. G.; Eychmüller, A.; Grätzel, M. *ACS Nano* **2012**, *6*, 3092.
- Shockley, W.; Queisser, H. J. *J. Appl. Phys.* **1961**, *32*, 510.
- Beard, M. C.; Midgett, A. G.; Hanna, M. C.; Luther, J. M.; Hughes, B. K.; Nozik, A. J. *Nano Lett.* **2010**, *10*, 3019.
- Nozik, A. J. *Nano Lett.* **2010**, *10*, 2735.
- Sze, S. M. *Physics of Semiconductor Devices*, 2nd ed.; Wiley-Interscience: New York, 1981.
- Choi, J. J.; Lim, Y.-F.; Santiago-Berrios, M. B.; Oh, M.; Hyun, B.-R.; Sun, L.; Bartnik, A. C.; Goedhart, A.; Malliaras, G. G.; Abruña, H. D.; Wise, F. W.; Hanrath, T. *Nano Lett.* **2009**, *9*, 3749.
- Leatherdale, C. A.; Kagan, C. R.; Morgan, N. Y.; Empedocles, S. A.; Kastner, M. A.; Bawendi, M. G. *Phys. Rev. B* **2000**, *62*, 2669.
- Choi, J. J.; Luria, J.; Hyun, B.-R.; Bartnik, A. C.; Sun, L.; Lim, Y.-F.; Marohn, J. A.; Wise, F. W.; Hanrath, T. *Nano Lett.* **2010**, *10*, 1805.
- Lee, J.-S.; Kovalenko, M. V.; Huang, J.; Chung, D. S.; Talapin, D. V. *Nat. Nanotechnol.* **2011**, *6*, 348.
- Guyot-Sionnest, P. *J. Phys. Chem. Lett.* **2012**, *3*, 1169.
- CRC Handbook of Chemistry and Physics*, 90th ed.; Lide, D. R., Ed.; CRC Press LLC: Boca Raton, FL, 2010.
- Ip, A. H.; Thon, S. M.; Hoogland, S.; Voznyy, O.; Zhitomirsky, D.; Debnath, R.; Levina, L.; Rollny, L. R.; Carey, G. H.; Fischer, A.; Kemp, K. W.; Kramer, I. J.; Ning, Z.; Labelle, A. J.; Chou, K. W.; Amassian, A.; Sargent, E. H. *Nat. Nanotechnol.* **2012**, *7*, 577.
- Liu, H.; Zhitomirsky, D.; Hoogland, S.; Tang, J.; Kramer, I. J.; Ning, Z.; Sargent, E. H. *Appl. Phys. Lett.* **2012**, *101*, 151112.
- Kang, M. S.; Sahu, A.; Norris, D. J.; Frisbie, C. D. *Nano Lett.* **2010**, *10*, 3727.
- Kang, M. S.; Sahu, A.; Norris, D. J.; Frisbie, C. D. *Nano Lett.* **2011**, *11*, 3887.
- Liu, Y.; Gibbs, M.; Puthussery, J.; Gaik, S.; Ihly, R.; Hillhouse, H. W.; Law, M. *Nano Lett.* **2010**, *10*, 1960.
- Kovalenko, M. V.; Scheele, M.; Talapin, D. V. *Science* **2009**, *324*, 1417.
- Chung, D. S.; Lee, J.-S.; Huang, J.; Nag, A.; Ithurria, S.; Talapin, D. V. *Nano Lett.* **2012**, *12*, 1813.
- Liu, Y.; Gibbs, M.; Perkins, C. L.; Tolentino, J.; Zarghami, M. H.; Bustamante, J.; Law, M. *Nano Lett.* **2011**, *11*, 5349.
- Etgar, L.; Park, J.; Barolo, C.; Nazeeruddin, M. K.; Grätzel, M. *ACS Appl. Mater. Interfaces* **2011**, *3*, 3264.
- Fu, W.; Qin, S.; Liu, L.; Kim, T.-H.; Hellstrom, S.; Wang, W.; Liang, W.; Bai, X.; Li, A.-P.; Wang, E. *Nano Lett.* **2011**, *11*, 1913.
- Williams, K. J.; Tisdale, W. A.; Leschkes, K. S.; Haugstad, G.; Norris, D. J.; Aydil, E. S.; Zhu, X.-Y. *ACS Nano* **2009**, *3*, 1532.
- Yang, J.; Hyun, B.-R.; Basile, A. J.; Wise, F. W. *ACS Nano* **2012**, *6*, 8120.
- Lutich, A. A.; Mauser, C.; Da Como, E.; Huang, J.; Vaneski, A.; Talapin, D. V.; Rogach, A. L.; Feldmann, J. *Nano Lett.* **2010**, *10*, 4646.
- Talgorn, E.; Abellon, R. D.; Kooyman, P. J.; Piris, J.; Savenije, T. J.; Goossens, A.; Houtepen, A. J.; Siebbeles, L. D. A. *ACS Nano* **2010**, *4*, 1723.
- Baranov, D.; Fiore, A.; van Huis, M.; Giannini, C.; Falqui, A.; Lafont, U.; Zandbergen, H.; Zanella, M.; Cingolani, R.; Manna, L. *Nano Lett.* **2010**, *10*, 743.
- Bodnarchuk, M. I.; Kovalenko, M. V.; Heiss, W.; Talapin, D. V. *J. Am. Chem. Soc.* **2010**, *132*, 11967.
- Choi, J. J.; Bian, K.; Baumgardner, W. J.; Smilgies, D.-M.; Hanrath, T. *Nano Lett.* **2012**, *12*, 4791.
- Hanrath, T. *J. Vac. Sci. Technol., A* **2012**, *30*, 030802.

- (62) Kovalenko, M. V.; Bodnarchuk, M. I.; Talapin, D. V. *J. Am. Chem. Soc.* **2010**, *132*, 15124.
- (63) Miszta, K.; Graaf, J. de; Bertoni, G.; Dorfs, D.; Brescia, R.; Marras, S.; Ceseracciu, L.; Cingolani, R.; Roij, R.; van Dijkstra, M.; Manna, L. *Nat. Mater.* **2011**, *10*, 872.
- (64) Park, J.; Zheng, H.; Lee, W. C.; Geissler, P. L.; Rabani, E.; Alivisatos, A. P. *ACS Nano* **2012**, *6*, 2078.
- (65) Rupich, S. M.; Talapin, D. V. *Nat. Mater.* **2011**, *10*, 815.
- (66) Shevchenko, E. V.; Talapin, D. V.; Kotov, N. A.; O'Brien, S.; Murray, C. B. *Nature* **2006**, *439*, 55.
- (67) Talapin, D. V.; Murray, C. B. *Science* **2005**, *310*, 86.
- (68) Talapin, D. V. *ACS Nano* **2008**, *2*, 1097.
- (69) Evers, W. H.; Goris, B.; Bals, S.; Casavola, M.; de Graaf, J.; Roij, R.; van Dijkstra, M.; Vanmaekelbergh, D. *Nano Lett.* **2013**, *13*, 2317.
- (70) Van Sark, W. G. J. H. M.; Frederix, P. L. T. M.; Van den Heuvel, D. J.; Gerritsen, H. C.; Bol, A. A.; van Lingen, J. N. J.; de Mello Donegá, C.; Meijerink, A. J. *Phys. Chem. B* **2001**, *105*, 8281.
- (71) Wang, X.; Qu, L.; Zhang, J.; Peng, X.; Xiao, M. *Nano Lett.* **2003**, *3*, 1103.
- (72) Hughes, B. K.; Ruddy, D. A.; Blackburn, J. L.; Smith, D. K.; Bergren, M. R.; Nozik, A. J.; Johnson, J. C.; Beard, M. C. *ACS Nano* **2012**, *6*, 5498.
- (73) Choi, H.; Ko, J.-H.; Kim, Y.-H.; Jeong, S. J. *Am. Chem. Soc.* **2013**, *135*, 5278.
- (74) Tang, J.; Wang, X.; Brzozowski, L.; Barkhouse, D. A. R.; Debnath, R.; Levina, L.; Sargent, E. H. *Adv. Mater.* **2010**, *22*, 1398.
- (75) Tang, J.; Brzozowski, L.; Barkhouse, D. A. R.; Wang, X.; Debnath, R.; Wolowiec, R.; Palmiano, E.; Levina, L.; Pattantyus-Abraham, A. G.; Jamakosmanovic, D.; Sargent, E. H. *ACS Nano* **2010**, *4*, 869.
- (76) Luther, J. M.; Gao, J.; Lloyd, M. T.; Semonin, O. E.; Beard, M. C.; Nozik, A. J. *Adv. Mater.* **2010**, *22*, 3704.
- (77) Gur, I.; Fromer, N. A.; Geier, M. L.; Alivisatos, A. P. *Science* **2005**, *310*, 462.
- (78) Wu, Y.; Wadia, C.; Ma, W.; Sadtler, B.; Alivisatos, A. P. *Nano Lett.* **2008**, *8*, 2551.
- (79) Talgorn, E.; Gao, Y.; Aerts, M.; Kunneman, L. T.; Schins, J. M.; Savenije, T. J.; Huis, M. A.; van Zant, H. S. J.; van der Houtepen, A. J.; Siebbeles, L. D. A. *Nat. Nanotechnol.* **2011**, *6*, 733.
- (80) Yu, D.; Wang, C.; Wehrenberg, B. L.; Guyot-Sionnest, P. *Phys. Rev. Lett.* **2004**, *92*, 216802.
- (81) Mentzel, T. S.; Porter, V. J.; Geyer, S.; MacLean, K.; Bawendi, M. G.; Kastner, M. A. *Phys. Rev. B* **2008**, *77*, 075316.
- (82) Liu, H.; Pourret, A.; Guyot-Sionnest, P. *ACS Nano* **2010**, *4*, 5211.
- (83) Kocherzhenko, A. A.; Grozema, F. C.; Vyrko, S. A.; Poklonski, N. A.; Siebbeles, L. D. A. *J. Phys. Chem. C* **2010**, *114*, 20424.
- (84) Barkhouse, D. A. R.; Pattantyus-Abraham, A. G.; Levina, L.; Sargent, E. H. *ACS Nano* **2008**, *2*, 2356.
- (85) Zhitomirsky, D.; Kramer, I. J.; Labelle, A. J.; Fischer, A.; Debnath, R.; Pan, J.; Bakr, O. M.; Sargent, E. H. *Nano Lett.* **2012**, *12*, 1007.
- (86) Zarghami, M. H.; Liu, Y.; Gibbs, M.; Gebremichael, E.; Webster, C.; Law, M. *ACS Nano* **2010**, *4*, 2475.
- (87) Voznyy, O. *J. Phys. Chem. C* **2011**, *115*, 15927.
- (88) Nelson, C. A.; Zhu, X.-Y. *J. Am. Chem. Soc.* **2012**, *134*, 7592.
- (89) Loef, R.; Houtepen, A. J.; Talgorn, E.; Schoonman, J.; Goossens, A. *Nano Lett.* **2009**, *9*, 856.
- (90) Köntges, M.; Reineke-Koch, R.; Nollet, P.; Beier, J.; Schäffler, R.; Parisi, J. *Thin Solid Films* **2002**, *403–404*, 280.
- (91) Nagpal, P.; Klimov, V. I. *Nat. Commun.* **2011**, *2*, 486.
- (92) Kramer, I. J.; Zhitomirsky, D.; Bass, J. D.; Rice, P. M.; Topuria, T.; Krupp, L.; Thon, S. M.; Ip, A. H.; Debnath, R.; Kim, H.-C.; Sargent, E. H. *Adv. Mater.* **2012**, *24*, 2315.
- (93) Tang, J.; Kemp, K. W.; Hoogland, S.; Jeong, K. S.; Liu, H.; Levina, L.; Furukawa, M.; Wang, X.; Debnath, R.; Cha, D.; Chou, K. W.; Fischer, A.; Amassian, A.; Asbury, J. B.; Sargent, E. H. *Nat. Mater.* **2011**, *10*, 765.
- (94) Jeong, K. S.; Tang, J.; Liu, H.; Kim, J.; Schaefer, A. W.; Kemp, K.; Levina, L.; Wang, X.; Hoogland, S.; Debnath, R.; Brzozowski, L.; Sargent, E. H.; Asbury, J. B. *ACS Nano* **2012**, *6*, 89.
- (95) Erslev, P. T.; Chen, H.-Y.; Gao, J.; Beard, M. C.; Frank, A. J.; van de Lagemaat, J.; Johnson, J. C.; Luther, J. M. *Phys. Rev. B* **2012**, *86*, 155313.
- (96) Urbach, F. *Phys. Rev.* **1953**, *92*, 1324.
- (97) Klar, T. A.; Franzl, T.; Rogach, A. L.; Feldmann, J. *Adv. Mater.* **2005**, *17*, 769.
- (98) Xu, F.; Ma, X.; Haughn, C. R.; Benavides, J.; Doty, M. F.; Cloutier, S. G. *ACS Nano* **2011**, *5*, 9950.
- (99) Franzl, T.; Klar, T. A.; Schietinger, S.; Rogach, A. L.; Feldmann, J. *Nano Lett.* **2004**, *4*, 1599.
- (100) Kramer, I. J.; Levina, L.; Debnath, R.; Zhitomirsky, D.; Sargent, E. H. *Nano Lett.* **2011**, *11*, 3701.
- (101) Graetzel, M.; Janssen, R. A. J.; Mitzi, D. B.; Sargent, E. H. *Nature* **2012**, *488*, 304.
- (102) Kemp, K. W.; Labelle, A. J.; Thon, S. M.; Ip, A. H.; Kramer, I. J.; Hoogland, S.; Sargent, E. H. *Adv. Energy Mater.* **2013**, *3*, 917.
- (103) Liu, H.; Tang, J.; Kramer, I. J.; Debnath, R.; Koleilat, G. I.; Wang, X.; Fisher, A.; Li, R.; Brzozowski, L.; Levina, L.; Sargent, E. H. *Adv. Mater.* **2011**, *23*, 3832.
- (104) Kamat, P. V.; Tvrđy, K.; Baker, D. R.; Radich, J. G. *Chem. Rev.* **2010**, *110*, 6664.
- (105) Greenham, N. C.; Peng, X.; Alivisatos, A. P. *Phys. Rev. B* **1996**, *54*, 17628.
- (106) Huynh, W. U.; Dittmer, J. J.; Alivisatos, A. P. *Science* **2002**, *295*, 2425.
- (107) Zaban, A.; Mičić, O. I.; Gregg, B. A.; Nozik, A. J. *Langmuir* **1998**, *14*, 3153.
- (108) Leschkes, K. S.; Divakar, R.; Basu, J.; Enache-Pommer, E.; Boercker, J. E.; Carter, C. B.; Kortshagen, U. R.; Norris, D. J.; Aydil, E. S. *Nano Lett.* **2007**, *7*, 1793.
- (109) Mora-Seró, I.; Giménez, S.; Moehl, T.; Fabregat-Santiago, F.; Lana-Villareal, T.; Gómez, R.; Bisquert, J. *Nanotechnology* **2008**, *19*, 424007.
- (110) Im, S. H.; Kim, H.; Kim, S. W.; Kim, S.-W.; Seok, S. I. *Energy Environ. Sci.* **2011**, *4*, 4181.
- (111) Im, S. H.; Kim, H.; Kim, S. W.; Kim, S.-W.; Seok, S. I. *Nanoscale* **2012**, *4*, 1581.
- (112) Guijarro, N.; Lana-Villareal, T.; Mora-Seró, I.; Bisquert, J.; Gómez, R. *J. Phys. Chem. C* **2009**, *113*, 4208.
- (113) Chen, J.; Song, J. L.; Sun, X. W.; Deng, W. Q.; Jiang, C. Y.; Lei, W.; Huang, J. H.; Liu, R. S. *Appl. Phys. Lett.* **2009**, *94*, 153115.
- (114) Lee, H.; Wang, M.; Chen, P.; Gamelin, D. R.; Zakeeruddin, S. M.; Grätzel, M.; Nazeeruddin, M. K. *Nano Lett.* **2009**, *9*, 4221.
- (115) Wijayantha, K. G. U.; Peter, L. M.; Otley, L. C. *Sol. Energy Mater. Sol. Cells* **2004**, *83*, 363.
- (116) Giménez, S.; Mora-Seró, I.; Macor, L.; Guijarro, N.; Lana-Villareal, T.; Gómez, R.; Diguna, L. J.; Shen, Q.; Toyoda, T.; Bisquert, J. *Nanotechnology* **2009**, *20*, 295204.
- (117) Weller, H. *Ber. Bunsen-Ges.* **1991**, *95*, 1361.
- (118) Vogel, R.; Hoyer, P.; Weller, H. *J. Phys. Chem.* **1994**, *98*, 3183.
- (119) Hoyer, P.; Könenkamp, R. *Appl. Phys. Lett.* **1995**, *66*, 349.
- (120) Liu, D.; Kamat, P. V. *J. Phys. Chem.* **1993**, *97*, 10769.
- (121) Niitsoo, O.; Sarkar, S. K.; Pejoux, C.; Rühle, S.; Cahen, D.; Hodes, G. *J. Photochem. Photobiol., A* **2006**, *181*, 306.
- (122) Lee, H.; Leventis, H. C.; Moon, S.-J.; Chen, P.; Ito, S.; Haque, S. A.; Torres, T.; Nüesch, F.; Geiger, T.; Zakeeruddin, S. M.; Grätzel, M.; Nazeeruddin, M. K. *Adv. Funct. Mater.* **2009**, *19*, 2735.
- (123) Santra, P. K.; Kamat, P. V. *J. Am. Chem. Soc.* **2012**, *134*, 2508.
- (124) Lee, J.-W.; Son, D.-Y.; Ahn, T. K.; Shin, H.-W.; Kim, I. Y.; Hwang, S.-J.; Ko, M. J.; Sul, S.; Han, H.; Park, N.-G. *Sci. Rep.* **2013**, *3*, 1050.
- (125) McDonald, S. A.; Konstantatos, G.; Zhang, S.; Cyr, P. W.; Klem, E. J. D.; Levina, L.; Sargent, E. H. *Nat. Mater.* **2005**, *4*, 138.
- (126) Maria, A.; Cyr, P. W.; Klem, E. J. D.; Levina, L.; Sargent, E. H. *Appl. Phys. Lett.* **2005**, *87*, 213112.
- (127) Schottky, W. *Z. Physik* **1942**, *118*, 539.

- (128) Klem, E. J. D.; MacNeil, D. D.; Cyr, P. W.; Levina, L.; Sargent, E. H. *Appl. Phys. Lett.* **2007**, *90*, 183113.
- (129) Koleilat, G. I.; Levina, L.; Shukla, H.; Myrskog, S. H.; Hinds, S.; Pattantyus-Abraham, A. G.; Sargent, E. H. *ACS Nano* **2008**, *2*, 833.
- (130) Johnston, K. W.; Pattantyus-Abraham, A. G.; Clifford, J. P.; Myrskog, S. H.; MacNeil, D. D.; Levina, L.; Sargent, E. H. *Appl. Phys. Lett.* **2008**, *92*, 151115.
- (131) Luther, J. M.; Law, M.; Beard, M. C.; Song, Q.; Reese, M. O.; Ellingson, R. J.; Nozik, A. J. *Nano Lett.* **2008**, *8*, 3488.
- (132) Ma, W.; Luther, J. M.; Zheng, H.; Wu, Y.; Alivisatos, A. P. *Nano Lett.* **2009**, *9*, 1699.
- (133) Debnath, R.; Tang, J.; Barkhouse, D. A.; Wang, X.; Pattantyus-Abraham, A. G.; Brzozowski, L.; Levina, L.; Sargent, E. H. *J. Am. Chem. Soc.* **2010**, *132*, 5952.
- (134) Ma, W.; Swisher, S. L.; Ewers, T.; Engel, J.; Ferry, V. E.; Atwater, H. A.; Alivisatos, A. P. *ACS Nano* **2011**, *5*, 8140.
- (135) Gao, J.; Perkins, C. L.; Luther, J. M.; Hanna, M. C.; Chen, H.-Y.; Semonin, O. E.; Nozik, A. J.; Ellingson, R. J.; Beard, M. C. *Nano Lett.* **2011**, *11*, 3263.
- (136) Gao, J.; Luther, J. M.; Semonin, O. E.; Ellingson, R. J.; Nozik, A. J.; Beard, M. C. *Nano Lett.* **2011**, *11*, 1002.
- (137) Tsang, S. W.; Fu, H.; Wang, R.; Lu, J.; Yu, K.; Tao, Y. *Appl. Phys. Lett.* **2009**, *95*, 183505.
- (138) Szendrei, K.; Gomulya, W.; Yarema, M.; Heiss, W.; Loi, M. A. *Appl. Phys. Lett.* **2010**, *97*, 203501.
- (139) Klem, E. J. D.; Gregory, C. W.; Cunningham, G. B.; Hall, S.; Temple, D. S.; Lewis, J. S. *Appl. Phys. Lett.* **2012**, *100*, 173109.
- (140) Hyun, B.-R.; Zhong, Y.-W.; Bartnik, A. C.; Sun, L.; Abruña, H. D.; Wise, F. W.; Goodreau, J. D.; Matthews, J. R.; Leslie, T. M.; Borrelli, N. F. *ACS Nano* **2008**, *2*, 2206.
- (141) Jasieniak, J.; Califano, M.; Watkins, S. E. *ACS Nano* **2011**, *5*, 5888.
- (142) Burgelman, M.; Nollet, P.; Degraeve, S. *Thin Solid Films* **2000**, *361–362*, 527.
- (143) Anderson, R. L. *IBM J. Res. Dev.* **1960**, *4*, 283.
- (144) O'Hayre, R.; Nanu, M.; Schoonman, J.; Goossens, A. *J. Phys. Chem. C* **2007**, *111*, 4809.
- (145) O'Regan, B.; Moser, J.; Anderson, M.; Graetzel, M. *J. Phys. Chem.* **1990**, *94*, 8720.
- (146) Zaban, A.; Meier, A.; Gregg, B. A. *J. Phys. Chem. B* **1997**, *101*, 7985.
- (147) Nakade, S.; Saito, Y.; Kubo, W.; Kanzaki, T.; Kitamura, T.; Wada, Y.; Yanagida, S. *Electrochem. Commun.* **2003**, *5*, 804.
- (148) Barkhouse, D. A. R.; Kramer, I. J.; Wang, X.; Sargent, E. H. *Opt. Express* **2010**, *18*, A451.
- (149) Von Roos, O. *J. Appl. Phys.* **1978**, *49*, 3503.
- (150) Brown, P. R.; Lunt, R. R.; Zhao, N.; Osedach, T. P.; Wanger, D. D.; Chang, L.-Y.; Bawendi, M. G.; Bulović, V. *Nano Lett.* **2011**, *11*, 2955.
- (151) Debnath, R.; Greiner, M. T.; Kramer, I. J.; Fischer, A.; Tang, J.; Barkhouse, D. A. R.; Wang, X.; Levina, L.; Lu, Z.-H.; Sargent, E. H. *Appl. Phys. Lett.* **2010**, *97*, 023109.
- (152) Wuister, S. F.; de Mello Donegá, C.; Meijerink, A. *J. Phys. Chem. B* **2004**, *108*, 17393.
- (153) Paz-Soldan, D.; Lee, A.; Thon, S. M.; Adachi, M. M.; Dong, H.; Maraghechi, P.; Yuan, M.; Labelle, A. J.; Hoogland, S.; Liu, K.; Kumacheva, E.; Sargent, E. H. *Nano Lett.* **2013**, *13*, 1502.
- (154) Koleilat, G. I.; Kramer, I. J.; Wong, C. T. O.; Thon, S. M.; Labelle, A. J.; Hoogland, S.; Sargent, E. H. *Sci. Rep.* **2013**, *3*, 2166.
- (155) Maraghechi, P.; Labelle, A. J.; Kirmani, A. R.; Lan, X.; Adachi, M. M.; Thon, S. M.; Hoogland, S.; Lee, A.; Ning, Z.; Fischer, A.; Amassian, A.; Sargent, E. H. *ACS Nano* **2013**, *7*, 6111.
- (156) Wolf, M. *Proc. IEEE* **1963**, *51*, 674.
- (157) Yan, H.; Lee, P.; Armstrong, N. R.; Graham, A.; Evmenenko, G. A.; Dutta, P.; Marks, T. J. *J. Am. Chem. Soc.* **2005**, *127*, 3172.
- (158) Peumans, P.; Forrest, S. R. *Appl. Phys. Lett.* **2001**, *79*, 126.
- (159) Brabec, C. J.; Shaheen, S. E.; Winder, C.; Sariciftci, N. S.; Denk, P. *Appl. Phys. Lett.* **2002**, *80*, 1288.
- (160) Koeppe, R.; Bossart, O.; Calzaferri, G.; Sariciftci, N. S. *Sol. Energy Mater. Sol. Cells* **2007**, *91*, 986.
- (161) Morales-Acevedo, A. *Sol. Energy* **2009**, *83*, 1466.
- (162) Tsakalakos, L. *Mater. Sci. Eng., R* **2008**, *62*, 175.
- (163) Weiss, E. A.; Chiechi, R. C.; Geyer, S. M.; Porter, V. J.; Bell, D. C.; Bawendi, M. G.; Whitesides, G. M. *J. Am. Chem. Soc.* **2008**, *130*, 74.
- (164) Kamat, P. V. *J. Phys. Chem. C* **2008**, *112*, 18737.
- (165) Hardin, B. E.; Hoke, E. T.; Armstrong, P. B.; Yum, J.-H.; Comte, P.; Torres, T.; Frechet, J. M. J.; Nazeeruddin, M. K.; Gratzel, M.; McGehee, M. D. *Nat. Photonics* **2009**, *3*, 406.
- (166) Han, J.-H.; Paulus, G. L. C.; Maruyama, R.; Heller, D. A.; Kim, W.-J.; Barone, P. W.; Lee, C. Y.; Choi, J. H.; Ham, M.-H.; Song, C.; Fantini, C.; Strano, M. S. *Nat. Mater.* **2010**, *9*, 833.
- (167) Shankar, K.; Feng, X.; Grimes, C. A. *ACS Nano* **2009**, *3*, 788.
- (168) Guha, S.; Yang, J.; Pawlikiewicz, A.; Glatfelter, T.; Ross, R.; Ovshinsky, S. R. *Appl. Phys. Lett.* **1989**, *54*, 2330.
- (169) Tikhomirov, G.; Hoogland, S.; Lee, P. E.; Fischer, A.; Sargent, E. H.; Kelley, S. O. *Nat. Nanotechnol.* **2011**, *6*, 485.
- (170) Leschkies, K. S.; Jacobs, A. G.; Norris, D. J.; Aydil, E. S. *Appl. Phys. Lett.* **2009**, *95*, 193103.
- (171) Barkhouse, D. A. R.; Debnath, R.; Kramer, I. J.; Zhitomirsky, D.; Pattantyus-Abraham, A. G.; Levina, L.; Etgar, L.; Grätzel, M.; Sargent, E. H. *Adv. Mater.* **2011**, *23*, 3134.
- (172) Bass, J. D.; Schaper, C. D.; Rettner, C. T.; Arellano, N.; Alharbi, F. H.; Miller, R. D.; Kim, H.-C. *ACS Nano* **2011**, *5*, 4065.
- (173) Lan, X.; Bai, J.; Masala, S.; Thon, S. M.; Ren, Y.; Kramer, I. J.; Hoogland, S.; Simchi, A.; Koleilat, G. I.; Paz-Soldan, D.; Ning, Z.; Labelle, A. J.; Kim, J. Y.; Jabbour, G.; Sargent, E. H. *Adv. Mater.* **2013**, *25*, 1769.
- (174) Jean, J.; Chang, S.; Brown, P. R.; Cheng, J. J.; Rekemeyer, P. H.; Bawendi, M. G.; Gradečak, S.; Bulović, V. *Adv. Mater.* **2013**, *25*, 2790.
- (175) Fan, Z.; Razavi, H.; Do, J.; Moriwaki, A.; Ergen, O.; Chueh, Y.-L.; Leu, P. W.; Ho, J. C.; Takahashi, T.; Reichertz, L. A.; Neale, S.; Yu, K.; Wu, M.; Ager, J. W.; Javey, A. *Nat. Mater.* **2009**, *8*, 648.
- (176) Van de Lagemaat, J.; Park, N.-G.; Frank, A. J. *J. Phys. Chem. B* **2000**, *104*, 2044.
- (177) Lee, Y. G.; Kang, C. G.; Jung, U. J.; Kim, J. J.; Hwang, H. J.; Chung, H.-J.; Seo, S.; Choi, R.; Lee, B. H. *Appl. Phys. Lett.* **2011**, *98*, 183508.
- (178) Konstantatos, G.; Levina, L.; Tang, J.; Sargent, E. H. *Nano Lett.* **2008**, *8*, 4002.
- (179) Rath, A. K.; Bernechea, M.; Martinez, L.; Konstantatos, G. *Adv. Mater.* **2011**, *23*, 3712.
- (180) Rath, A. K.; Bernechea, M.; Martinez, L.; de Arquer, F. P. G.; Osmond, J.; Konstantatos, G. *Nat. Photonics* **2012**, *6*, 529.
- (181) MacDonald, B. I.; Martucci, A.; Rubanov, S.; Watkins, S. E.; Mulvaney, P.; Jasieniak, J. J. *ACS Nano* **2012**, *6*, 5995.
- (182) Noone, K. M.; Strein, E.; Anderson, N. C.; Wu, P.-T.; Jenekhe, S. A.; Ginger, D. S. *Nano Lett.* **2010**, *10*, 2635.
- (183) Ehrler, B.; Wilson, M. W. B.; Rao, A.; Friend, R. H.; Greenham, N. C. *Nano Lett.* **2012**, *12*, 1053.
- (184) Yu, D.; Wang, C.; Guyot-Sionnest, P. *Science* **2003**, *300*, 1277.
- (185) Buonsanti, R.; Milliron, D. J. *Chem. Mater.* **2013**, *25*, 1305.
- (186) Norris, D. J.; Efros, A. L.; Erwin, S. C. *Science* **2008**, *319*, 1776.
- (187) Mocatta, D.; Cohen, G.; Schattner, J.; Millo, O.; Rabani, E.; Banin, U. *Science* **2011**, *332*, 77.
- (188) Gunawan, A. A.; Mkhoyan, K. A.; Wills, A. W.; Thomas, M. G.; Norris, D. J. *Nano Lett.* **2011**, *11*, 5553.
- (189) Erwin, S. C.; Zu, L.; Haftel, M. I.; Efros, A. L.; Kennedy, T. A.; Norris, D. J. *Nature* **2005**, *436*, 91.
- (190) Engel, J. H.; Surendranath, Y.; Alivisatos, A. P. *J. Am. Chem. Soc.* **2012**, *134*, 13200.
- (191) Shim, M.; Guyot-Sionnest, P. *Nature* **2000**, *407*, 981.
- (192) Nag, A.; Chung, D. S.; Dolzhenkov, D. S.; Dimitrijevic, N. M.; Chattopadhyay, S.; Shibata, T.; Talapin, D. V. *J. Am. Chem. Soc.* **2012**, *134*, 13604.
- (193) Voznyy, O.; Zhitomirsky, D.; Stadler, P.; Ning, Z.; Hoogland, S.; Sargent, E. H. *ACS Nano* **2012**, *6*, 8448.

- (194) Tang, J.; Liu, H.; Zhitomirsky, D.; Hoogland, S.; Wang, X.; Furukawa, M.; Levina, L.; Sargent, E. H. *Nano Lett.* **2012**, *12*, 4889.
- (195) Zhitomirsky, D.; Furukawa, M.; Tang, J.; Stadler, P.; Hoogland, S.; Voznyy, O.; Liu, H.; Sargent, E. H. *Adv. Mater.* **2012**, *24*, 6181.
- (196) Ning, Z.; Ren, Y.; Hoogland, S.; Voznyy, O.; Levina, L.; Stadler, P.; Lan, X.; Zhitomirsky, D.; Sargent, E. H. *Adv. Mater.* **2012**, *24*, 6295.
- (197) Ning, Z.; Zhitomirsky, D.; Adinolfi, V.; Sutherland, B.; Xu, J.; Voznyy, O.; Maraghechi, P.; Lan, X.; Hoogland, S.; Ren, Y.; Sargent, E. H. *Adv. Mater.* **2013**, *25*, 1719.
- (198) Choi, J. J.; Wenger, W. N.; Hoffman, R. S.; Lim, Y.-F.; Luria, J.; Jasieniak, J.; Marohn, J. A.; Hanrath, T. *Adv. Mater.* **2011**, *23*, 3144.
- (199) Wang, X.; Koleilat, G. I.; Tang, J.; Liu, H.; Kramer, I. J.; Debnath, R.; Brzozowski, L.; Barkhouse, D. A. R.; Levina, L.; Hoogland, S.; Sargent, E. H. *Nat. Photonics* **2011**, *5*, 480.
- (200) Koleilat, G. I.; Wang, X.; Sargent, E. H. *Nano Lett.* **2012**, *12*, 3043.
- (201) Wang, X.; Koleilat, G. I.; Fischer, A.; Tang, J.; Debnath, R.; Levina, L.; Sargent, E. H. *ACS Appl. Mater. Interfaces* **2011**, *3*, 3792.
- (202) Koleilat, G. I.; Wang, X.; Labelle, A. J.; Ip, A. H.; Carey, G. H.; Fischer, A.; Levina, L.; Brzozowski, L.; Sargent, E. H. *Nano Lett.* **2011**, *11*, 5173.
- (203) Ellingson, R. J.; Beard, M. C.; Johnson, J. C.; Yu, P.; Micic, O. I.; Nozik, A. J.; Shabaev, A.; Efros, A. L. *Nano Lett.* **2005**, *5*, 865.
- (204) Beard, M. C.; Luther, J. M.; Semonin, O. E.; Nozik, A. J. *Acc. Chem. Res.* **2012**, *46*, 1252.
- (205) Nozik, A. J. *Chem. Phys. Lett.* **2008**, *457*, 3.
- (206) Pelouch, W. S.; Ellingson, R. J.; Powers, P. E.; Tang, C. L.; Szymd, D. M.; Nozik, A. J. *Phys. Rev. B* **1992**, *45*, 1450.
- (207) Rosenwaks, Y.; Hanna, M. C.; Levi, D. H.; Szymd, D. M.; Ahrenkiel, R. K.; Nozik, A. J. *Phys. Rev. B* **1993**, *48*, 14675.
- (208) Bockelmann, U.; Bastard, G. *Phys. Rev. B* **1990**, *42*, 8947.
- (209) Benisty, H.; Sotomayor-Torrès, C. M.; Weisbuch, C. *Phys. Rev. B* **1991**, *44*, 10945.
- (210) Ross, R. T.; Nozik, A. J. *J. Appl. Phys.* **1982**, *53*, 3813.
- (211) Würfel, P. *Sol. Energy Mater. Sol. Cells* **1997**, *46*, 43.
- (212) König, D.; Casalenuovo, K.; Takeda, Y.; Conibeer, G.; Guillemoles, J. F.; Patterson, R.; Huang, L. M.; Green, M. A. *Phys. E* **2010**, *42*, 2862.
- (213) Takeda, Y.; Ito, T.; Motohiro, T.; König, D.; Shrestha, S.; Conibeer, G. *J. Appl. Phys.* **2009**, *105*, 074905.
- (214) Green, M. A.; Conibeer, G.; König, D.; Shrestha, S.; Huang, S.; Aliberti, P.; Treiber, L.; Patterson, R.; Veettil, B. P.; Hsieh, A.; Feng, Y.; Luque, A.; Marti, A.; Linares, P. G.; Cánovas, E.; Antolín, E.; Fuentes Marrón, D.; Tablero, C.; Hernández, E.; Guillemoles, J.-F.; Huang, L.; Le Bris, A.; Schmidt, T.; Clady, R.; Tayebjee, M. *35th IEEE Photovoltaic Specialists Conference (PVSC)*, Honolulu, HI, June 2010.
- (215) Hendry, E.; Koeberg, M.; Wang, F.; Zhang, H.; deMello Donegá, C.; Vanmaekelbergh, D.; Bonn, M. *Phys. Rev. Lett.* **2006**, *96*, 057408.
- (216) Pandey, A.; Guyot-Sionnest, P. *Science* **2008**, *322*, 929.
- (217) Tisdale, W. A.; Williams, K. J.; Timp, B. A.; Norris, D. J.; Aydil, E. S.; Zhu, X.-Y. *Science* **2010**, *328*, 1543.
- (218) Guijarro, N.; Lana-Villarreal, T.; Lutz, T.; Haque, S. A.; Gómez, R. *J. Phys. Chem. Lett.* **2012**, *3*, 3367.
- (219) Kolodinski, S.; Werner, J. H.; Wittchen, T.; Queisser, H. J. *Appl. Phys. Lett.* **1993**, *63*, 2405.
- (220) Werner, J. H.; Kolodinski, S.; Queisser, H. J. *Phys. Rev. Lett.* **1994**, *72*, 3851.
- (221) Hillhouse, H. W.; Beard, M. C. *Curr. Opin. Colloid Interface Sci.* **2009**, *14*, 245.
- (222) Sambur, J. B.; Novet, T.; Parkinson, B. A. *Science* **2010**, *330*, 63.
- (223) Semonin, O. E.; Luther, J. M.; Choi, S.; Chen, H.-Y.; Gao, J.; Nozik, A. J.; Beard, M. C. *Science* **2011**, *334*, 1530.
- (224) Cragg, G. E.; Efros, A. L. *Nano Lett.* **2010**, *10*, 313.
- (225) Klimov, V. I.; McBranch, D. W.; Leatherdale, C. A.; Bawendi, M. G. *Phys. Rev. B* **1999**, *60*, 13740.
- (226) Klimov, V. I.; McGuire, J. A.; Schaller, R. D.; Rupasov, V. I. *Phys. Rev. B* **2008**, *77*, 195324.
- (227) Klimov, V. I.; Mikhailovsky, A. A.; McBranch, D. W.; Leatherdale, C. A.; Bawendi, M. G. *Science* **2000**, *287*, 1011.
- (228) Klimov, V. I.; Mikhailovsky, A. A.; Xu, S.; Malko, A.; Hollingsworth, J. A.; Leatherdale, C. A.; Eisler, H.-J.; Bawendi, M. G. *Science* **2000**, *290*, 314.
- (229) Klimov, V. I.; McBranch, D. W. *Phys. Rev. Lett.* **1998**, *80*, 4028.
- (230) Korkusinski, M.; Voznyy, O.; Hawrylak, P. *Phys. Rev. B* **2011**, *84*, 155327.
- (231) Robel, I.; Gresback, R.; Kortshagen, U.; Schaller, R. D.; Klimov, V. I. *Phys. Rev. Lett.* **2009**, *102*, 177404.
- (232) McGuire, J. A.; Joo, J.; Pietryga, J. M.; Schaller, R. D.; Klimov, V. I. *Acc. Chem. Res.* **2008**, *41*, 1810.
- (233) Stewart, J. T.; Padilha, L. A.; Qazilbash, M. M.; Pietryga, J. M.; Midgett, A. G.; Luther, J. M.; Beard, M. C.; Nozik, A. J.; Klimov, V. I. *Nano Lett.* **2012**, *12*, 622.
- (234) Gdor, I.; Sachs, H.; Roitblat, A.; Strasfeld, D. B.; Bawendi, M. G.; Ruhman, S. *ACS Nano* **2012**, *6*, 3269.
- (235) Nair, G.; Chang, L.-Y.; Geyer, S. M.; Bawendi, M. G. *Nano Lett.* **2011**, *11*, 2145.
- (236) Nair, G.; Bawendi, M. G. *Phys. Rev. B* **2007**, *76*, 081304.
- (237) Kambhampati, P. *Acc. Chem. Res.* **2011**, *44*, 1.
- (238) Ben-Lulu, M.; Mocatta, D.; Bonn, M.; Banin, U.; Ruhman, S. *Nano Lett.* **2008**, *8*, 1207.
- (239) Pijpers, J. J. H.; Hendry, E.; Milder, M. T. W.; Fanciulli, R.; Savolainen, J.; Herek, J. L.; Vanmaekelbergh, D.; Ruhman, S.; Mocatta, D.; Oron, D.; Aharoni, A.; Banin, U.; Bonn, M. *J. Phys. Chem. C* **2007**, *111*, 4146.
- (240) Law, M.; Beard, M. C.; Choi, S.; Luther, J. M.; Hanna, M. C.; Nozik, A. J. *Nano Lett.* **2008**, *8*, 3904.
- (241) McGuire, J. A.; Sykora, M.; Joo, J.; Pietryga, J. M.; Klimov, V. I. *Nano Lett.* **2010**, *10*, 2049.
- (242) Sykora, M.; Kuposov, A. Y.; McGuire, J. A.; Schulze, R. K.; Tretiak, O.; Pietryga, J. M.; Klimov, V. I. *ACS Nano* **2010**, *4*, 2021.
- (243) Miaja-Avila, L.; Tritsch, J. R.; Wolcott, A.; Chan, W.-L.; Nelson, C. A.; Zhu, X.-Y. *Nano Lett.* **2012**, *12*, 1588.
- (244) Schaller, R. D.; Klimov, V. I. *Phys. Rev. Lett.* **2004**, *92*, 186601.
- (245) Schaller, R. D.; Agranovich, V. M.; Klimov, V. I. *Nat. Phys.* **2005**, *1*, 189.
- (246) Schaller, R. D.; Sykora, M.; Pietryga, J. M.; Klimov, V. I. *Nano Lett.* **2006**, *6*, 424.
- (247) Trinh, M. T.; Limpens, R.; Boer, W. D. A. M. de; Schins, J. M.; Siebbeles, L. D. A.; Gregorkiewicz, T. *Nat. Photonics* **2012**, *6*, 316.
- (248) Witzel, W. M.; Shabaev, A.; Hellberg, C. S.; Jacobs, V. L.; Efros, A. L. *Phys. Rev. Lett.* **2010**, *105*, 137401.
- (249) Huang, J.; Huang, Z.; Yang, Y.; Zhu, H.; Lian, T. *J. Am. Chem. Soc.* **2010**, *132*, 4858.
- (250) Yang, Y.; Rodríguez-Córdoba, W.; Lian, T. *Nano Lett.* **2012**, *12*, 4235.
- (251) Binks, D. J. *Phys. Chem. Chem. Phys.* **2011**, *13*, 12693.
- (252) Hanna, M. C.; Beard, M. C.; Nozik, A. J. *J. Phys. Chem. Lett.* **2012**, *3*, 2857.
- (253) Zhu, H.; Song, N.; Lian, T. *J. Am. Chem. Soc.* **2011**, *133*, 8762.
- (254) Zhu, H.; Song, N.; Rodríguez-Córdoba, W.; Lian, T. *J. Am. Chem. Soc.* **2012**, *134*, 4250.
- (255) Aerts, M.; Suchand Sandeep, C. S.; Gao, Y.; Savenije, T. J.; Schins, J. M.; Houtepen, A. J.; Kinge, S.; Siebbeles, L. D. A. *Nano Lett.* **2011**, *11*, 4485.
- (256) Cunningham, P. D.; Boercker, J. E.; Foos, E. E.; Lumb, M. P.; Smith, A. R.; Tischler, J. G.; Melinger, J. S. *Nano Lett.* **2011**, *11*, 3476.
- (257) Sukhovatkin, V.; Hinds, S.; Brzozowski, L.; Sargent, E. H. *Science* **2009**, *324*, 1542.